Article:
Wang, R, Yang, Y, Jing, Y et al. (32 more authors) (2021) Molecular mechanisms of mutualistic and antagonistic interactions in a plant–pollinator association. Nature Ecology & Evolution, 5 (7). pp. 974-986. ISSN 2397-334X

https://doi.org/10.1038/s41559-021-01469-1

Molecular mechanisms of mutualistic and antagonistic interactions in a plant-pollinator association

Rong Wang[1,20†], Yang Yang[1†], Yi Jing[2†], Simon T. Segar[3†], Yu Zhang[1], Gang Wang[4], Jin Chen[4], Qing-Feng Liu[2], Shan Chen[1], Yan Chen[5], Astrid Cruaud[6], Yuan-Yuan Ding[1], Derek W. Dunn[7], Qiang Gao[2], Philip M. Gilmartin[8], Kai Jiang[1], Finn Kjellberg[9], Hong-Qing Li[10], Yuan-Yuan Li[1], Jian-Quan Liu[11], Min Liu[12], Carlos A. Machado[13], Ray Ming[14], Jean-Yves Rasplus[6], Xin Tong[1], Ping Wen[4], Huan-Ming Yang[2], Jing-Jun Yang[1], Ye Yin[2], Xing-Tan Zhang[15], Yuan-Ye Zhang[16], Hui Yu[17,18*], Zhen Yue[2*], Stephen G. Compton[19*], Xiao-Yong Chen[1,20*]

[1] Zhejiang Tiantong Forest Ecosystem National Observation and Research Station, Shanghai Key Lab for Urban Ecological Processes and Eco-Restoration, School of Ecological and Environmental Sciences, East China Normal University, Shanghai 200241, China

[2]BGI Genomics, BGI-Shenzhen, Shenzhen 518083, China

[3]Agriculture & Environment Department, Harper Adams University, Newport, TF10 8NB, United Kingdom

[4]CAS Key Laboratory of Tropical Forest Ecology, Xishuangbanna Tropical Botanical Garden, Chinese Academy of Sciences, Mengla, Yunnan Province 666303, China

[5]Ecological Security and Protection Key Laboratory of Sichuan Province, Mianyang Normal University, Mianyang 621000, China

[6]INRAE, UMR1062 CBGP, F-34988 Montferrier-sur-Lez, France

[7]College of Life Sciences, Northwest University, Xi'an, Shaanxi 710069, China

[8]Department of Biological and Marine Science, University of Hull, Hull HU6 7RX, UK

[9]CEFE, CNRS, Univ Montpellier, Univ Paul Valéry Montpellier, EPHE, IRD, France

[10]School of Life Sciences, East China Normal University, Shanghai 200241, China

[11]Key Laboratory of Bio-resource and Eco-environment of Ministry of Education, College of Life Sciences, Sichuan University, Chengdu 610065, China.

[12]School of Life Sciences, Guangzhou University, Guangzhou 510006, China

[13]Department of Biology, University of Maryland, College Park, MD 20742, The United States of America

[14]Department of Plant Biology, University of Illinois at Urbana-Champaign, Urbana, IL 61801, USA

[15]Center for Genomics and Biotechnology, Fujian Provincial Key Laboratory of Haixia Applied Plant Systems Biology, Key Laboratory of Genetics, Breeding and Multiple Utilization of Corps, Ministry of Education, Fujian Agriculture and Forestry University, Fuzhou 350002, China.

[16]Key Laboratory of the Ministry of Education for Coastal and Wetland Ecosystems, College of the Environment and Ecology, Xiamen University, Xiamen, Fujian 361102, China

[17]Key Laboratory of Plant Resource Conservation and Sustainable Utilization, South China Botanical Garden, Chinese Academy of Sciences, Guangzhou 510650, China

[18]School of Life Sciences, Qufu Normal University, Qufu Shandong, 273165, China

[19]School of Biology, University of Leeds, Leeds LS2 9JT, UK

[20]Shanghai Institute of Pollution Control and Ecological Security, Shanghai 200092, China

† These authors contributed equally to this work.

* Co-corresponding authors.

E-mail: xychen@des.ecnu.edu.cn (X.-Y.C.); yuhui@scib.ac.cn (H.Y.);

S.G.A.Compton@leeds.ac.uk (S.G.C.); yuezhen@bgi.com (Z.Y.)

Abstract

Many insects metamorphose from antagonistic larvae into mutualistic adult pollinators, with reciprocal adaptation leading to specialized insect-plant associations. It remains unknown how such interactions are established at molecular level. Here we assemble high-quality genomes of a fig species, *Ficus pumila* var. *pumila*, and its specific pollinating wasp, *Wiebesia pumilae*. We combine multi-omics with validation experiments to reveal molecular mechanisms underlying this specialized interaction. In the plant, we identify the specific compound attracting pollinators and validate the function of several key genes regulating its biosynthesis. In the pollinator, we find a highly reduced number of odorant-binding protein (OBP) genes and an OBP mainly binding the attractant. During antagonistic interaction, we find similar chemical profiles and turnovers throughout the development of galled ovules and seeds, and a significant contraction of detoxification-related gene families in the pollinator. Our study identifies some key genes bridging coevolved mutualists, establishing expectations for more diffuse insect-pollinator systems.

Keywords

Multi-omics, plant-pollinator mutualism, insect-host identification, pollinator adaptation to host plant, gene for gene coadaptation

Introduction

Evolutionary adaptation fuels the genetic diversification of living organisms, driving speciation and emergent biodiversity[1,2]. However, in contrast to adaptation to abiotic conditions[3-5], it remains unclear how species adapt to reciprocally evolving biotic factors at the molecular level. This reflects the difficulty of identifying the traits linking interspecific interactions in a dynamic selective landscape. The high diversity of phytophagous insects and angiosperms is believed to be the result of coevolution, in part driven by ongoing insect-plant arms races[6,7]. Many herbivorous insects are also responsible for mediating gene flow between plant populations, often occurring as both antagonistic (i.e., herbivorous) larvae and mutualistic pollinating adults[8]. Selection by multiple agents associated with herbivorous/pollinating insects acts on floral traits to both deter herbivores and attract pollinators[9], making it difficult to separate mechanistic processes in many plant-pollinator systems. Tightly co-evolved species often have more apparent interacting traits, which provide an excellent testing ground for exploring coadaptation.

The obligate mutualisms comprising ~800 species from the genus *Ficus* (Moraceae) and their host specific pollinating wasps (fig wasps; Hymenoptera, Agaonidae) form a classical example of coevolution and contribute greatly to ecosystem functioning, biodiversity and agriculture[10,11]. Both mutualists have evolved strict correspondence in morphological, metabolic and life history traits[10,12]. The plants reward the larvae of pollinating wasps with nutrition and protection, and each mutualist wasp species is both pollinator and herbivore[12]. Each individual wasp

97 spends the majority of its lifespan at the larval stage (from three weeks up to nine
98 months) and develops inside a single galled ovule of a female floret located inside the
99 enclosed inflorescences characteristic of the genus (figs or 'syconia')[13-15] (Fig. 1a).
100 There are two predominant types of breeding systems in *Ficus* species, monoecy and
101 dioecy[16]. In monoecious figs, each fig produces female florets that can be either
102 pollinated or galled by pollinator larvae. In dioecious species, only the female florets
103 (feeder florets) in figs of functional male trees support the development of pollinator
104 offspring; figs growing on female trees attract pollinators to fertilize the female florets
105 (seed florets) that do not support wasp development (Fig. 1a). Upon locating host figs,
106 adult female wasps must crawl through a narrow passage usually lined by bracts (the
107 ostiole), into a dark central lumen where they typically remain trapped following
108 oviposition and/or pollination. Short lived (usually shorter than three days) adult
109 wasps do not feed[10].

110 Central to mediating these species-specific interactions are plant-emitted volatile
111 organic compounds (VOCs), which guide adult female wasps to precisely identify and
112 locate host figs[13,14,17-21]. Moreover, the high-quality genomes of a *Ficus* species and its
113 pollinating wasp (*Ficus microcarpa* and *Eupristina verticillata*) have been recently
114 reported[11], which create a basis for exploring how these pollinators identify host figs
115 at the molecular level. However, to date the key attractive VOCs have only been
116 explicitly identified in a small number of fig-pollinator mutualisms[17,18], and the
117 underlying molecular mechanisms determining host-specific signaling and insect
118 attraction remain unknown.

Once the problem of host identification has been overcome, pollinator larvae must also survive and develop under a set of unique conditions inside galled ovules that support their development (Fig. 1a). While figs can defend against herbivores from a wide range of taxa[22], it is unclear how pollinator larvae cope with plant defensive chemicals inside the galled ovules during this antagonistic phase of mutualism. One possible explanation is that galling behavior may activate the plant reproductive program in galled tissues, so that galling insects can avoid the strong chemical defenses induced by stress reaction when they utilize plant nutrients[23-25]. To test whether the reproductive program is activated in galled ovules, it is necessary to compare between the chemical profiles of galled ovules and seeds. We also expect that such adaptation to a specialized environment must leave molecular footprints in pollinator genome, for example contracted detoxification-related gene families[26,27].

Here we focused on a fig-pollinator mutualism comprising a dioecious *Ficus* species *Ficus pumila* var. *pumila*[28] and its specific pollinator *Wiebesia pumilae*[29] (Fig. 1a). We used multi-omics in combination with validation experiments to unravel the key molecular mechanisms contributing to the antagonistic and the mutualistic interactions in this system. We determined the specific attractive VOC and several key genes relevant to its biosynthesis. We identified the corresponding responses in the odorant-binding protein (OBP) genes in the pollinator genome and an OBP mainly binding the attractant. During the antagonistic phase, we found a similar turnover of secondary metabolites when female florets developed into either galled ovules or seeds, and almost identical chemical profiles between these two tissues. It implies that

the galled ovules may develop like seeds. A contraction of detoxification-related gene families was found in the pollinator genome, providing insights into the fig-pollinator coadaptation during antagonistic interaction.

Results

Assembly of genomes and evolution

To provide high-quality reference genomes for transcriptomic and proteomic analyses, we assembled genomes of *F. pumila* var. *pumila* and *W. pumilae* using a combination of Illumina and PacBio sequencing technologies (Supplementary Table 1; see Methods). The assembled genomes were 315.7 Mb (contig N50 of 2.3 Mb) for the plant and 318.2 Mb (contig N50 of 10.9 Mb) for the pollinator (Table 1 and Supplementary Table 2). Using the uniquely mapped reads produced by the high-throughput chromatin conformation capture (Hi-C) technique (Supplementary Tables 1, 2), we generated Hi-C-based physical maps composed of 13 and 6 pseudo-chromosomes, with 96.6% (305 Mb) and 99.8% (318 Mb) of the assembled genomes anchored to the pseudo-chromosomes (Table 1 and Supplementary Fig. 1). The scaffold N50 of the assembled genomes were 22.4 Mb and 59.4 Mb, and the pseudo-chromosomes included 97.1% (27,378) and 99.8% (12,292) of protein-coding genes (Table 1). Genome annotation results showed that the structures and functions of 25,905 and 12,305 protein-coding genes were annotated in the two genomes (Supplementary Figs. 2 and Supplementary Tables 3-5). BUSCO quality analysis of annotation showed that 92.4% of 1375 conserved plant genes and 91.3% of 4,415 Hymenoptera genes have complete coverage (Supplementary Table 3).

163 The protein-coding genes of *F. pumila* var. *pumila* and *W. pumilae* were clustered
164 into 15,631 and 7,969 gene families (Supplementary Fig. 3 and Supplementary Table
165 6). Analysis of comparative genomics using the genomes of 13 Angiosperm species
166 including *F. pumila* var. *pumila* and three congeneric species (*Ficus hispida*[11], *Ficus*
167 *microcarpa*[11] and *Ficus carica*[16]) showed that in the common ancestors of the four
168 *Ficus* species, 1,473 gene families had contracted and 888 gene families had
169 expanded. Phylogenetic reconstruction revealed that *F. hispida* is more closely related
170 to *F. pumila var. pumila* than the other two *Ficus* species (Supplementary Fig. 4a). In
171 the analysis of comparative genomics using the genomes of 11 arthropod species
172 containing *W. pumilae* and two other pollinator wasp species (*Ceratosolen solmsi*[11]
173 and *Eupristina verticillata*[27]), we found 48 expanded and 1261 contracted gene
174 families in the common ancestors of three pollinating wasp species. We recovered a
175 group containing *E. verticillata* and *W. pumilae* with *C. solmsi* as its sibling
176 (Supplementary Fig. 4b). There was no evidence for recent whole-genome duplication
177 in the plant, and only a few small segments (total length of 1.3 Mb) were found to be
178 duplicated in the pollinator genome (Supplementary Fig. 5).

179 **Attractive compound forming fig-pollinator identification**

180 At the receptive stage, figs release VOCs containing critical compound(s)
181 attracting their pollinating wasps (Fig. 1a). To determine the attractive compound(s),
182 we collected VOCs from functional male and female figs of *F. pumila* var. *pumila* at
183 the pre-repetitive and the receptive stages using the dynamic headspace sampling
184 (DHS) approach, and identified a total of 70 compounds (Fig. 1a and Supplementary

Tables 7, 8). Only three (linalool, nonanal and decanal) of these compounds were found to elicit physiological responses of adult females of *W. pumilae* (Fig. 1b, c), of which only decanal was emitted exclusively at the receptive stage (Supplementary Table 8). We then conducted behavioral preference tests among the three compounds using 50 female pollinating wasps in each testing group. The wasps showed a significantly greater preference for decanal than the control and a significantly reduced preference for nonanal than the control, with a similar preference between decanal and a nonanal-decanal blend (Fig. 1d and Supplementary Table 9). These results demonstrate that the VOC compound decanal, emitted by *F. pumila* var. *pumila* figs at the receptive stage, functions to attract the pollinating wasp *W. pumilae*.

Molecular mechanisms of specific host identification

To identify the molecular mechanisms underlying the behavioral responses of *W. pumilae* to the VOCs emitted by its host figs, we annotated the four gene families involved in insect olfaction[30]. Across these gene families, *W. pumilae*, *E. verticillata* and *C. solmsi* consistently have lower numbers of genes, and, in particular, the number of odorant-binding protein (OBP) genes is significantly lower than less host-specific insects (Fig. 2a). Phylogenetic and synteny analysis including genomes of the three pollinating wasp species and the distantly related *Nasonia vitripennis* showed that most OBP genes in the pollinating wasp species displayed strong homology and that the small number of OBP genes resulted from gene loss and infrequent tandem duplication (Supplementary Figs. 6a, 7a). There were apparent differences in motif

structure among OBPs in six of the ten syntenic blocks (Supplementary Fig. 6b). The general contraction in OBP genes and frequent changes in motif structure of homologous OBPs among pollinating wasp species may be expected given their high host specificity and different VOC cues used for detecting host figs.

Among the 12 OBP genes of *W. pumilae*, transcriptome and proteome evidence showed that all genes were transcribed but only seven are translated into detectable proteins in adult females (Fig. 2b, Supplementary Fig. 8 and Supplementary Table 7). There were no proteins with significant differences in quantity (PSDs) and differentially expressed genes (DEGs) between the control and the VOCs-contacting treatment (Supplementary Table 10).

To explore functions of *W. pumilae* OBPs, we predicted motif structures of OBPs and compared them with the OBPs in *Adelphocoris lineolatus*[31] and *Culex quinquefasciatus*[32], known to have decanal or nonanal binding activity. Among the seven OBPs with detectable protein products, WpumOBP2 shows similar structure to the known decanal-binding protein and WpumOBP11 is similar to the known nonanal-binding protein (Fig. 2c and Supplementary Fig. 9). To validate the functions of WpumOBP2 and WpumOBP11, we produced the recombinant proteins for these two OBPs and measured their binding affinity to decanal and nonanal using surface plasmon resonance (SPR) experiments. Consistent with the prediction, the experiments revealed considerably lower K_D (representing much higher binding affinity) of WpumOPB2 to decanal than to nonanal and far lower K_D of WpumOBP11 to nonanal than to decanal, and thus demonstrate the high binding affinity of these two

OBPs to the corresponding compounds (Fig 2d, Supplementary Fig. 10 and Supplementary Table 11). Therefore, these results provide solid evidence that WpumOBP2 is the main binding protein to the attractant, and pollination of *F. pumila var. pumila* by *W. pumilae* is initiated by the binding of decanal with WpumOPB2.

Regulation of gene expression in attractant biosynthesis

To identify the tissue for attractant emission within figs, we measured the concentration of decanal emitted by ostiolar tissues and female florets at the receptive stage from both sexes of *F. pumila* var. *pumila* (Fig. 1a) using DHS, as previous studies from other species suggested VOCs are mainly released from these tissues[13,20]. The concentration of collected decanal in ostiolar tissues was 3.13 ± 1.11 pg/g, which was 9.1 times as that in female florets (0.34 ± 0.05 pg/g) (Pairwise T Test: df=9, t=6.02, p=0.002). Thus, the results revealed that decanal was predominantly emitted by ostiolar tissues at a similar concentration between sexes (T Test: df=4, t=0.20, p=0.858 in ostiolar tissues; df=4, t=0.24, p=0.826 in female florets).

To identify key genes involved in the biosynthesis of decanal, we conducted transcriptome and proteome analyses on ostiolar tissues collected at the pre-receptive and the receptive stages (Supplementary Table 7). The biosynthesis of decanal and nonanal is involved in the pathways of fatty acid biosynthesis (ko00061), elongation (ko00062) and metabolism (ko00071 and ko00592) (Fig. 3a)[33,34]. Genes in these pathways showed similar patterns of expression between transcriptome and proteome data (Supplementary Fig. 11 and Supplementary Table 12). Comparing the receptive

with the pre-receptive stage, we detected a total of eight PSDs (Fig. 3b), likely facilitating the biosynthesis of decanal and suppressing the biosynthesis of nonanal at the receptive stage (Fig. 3a). Down-regulated PSDs included two ACSLs (long-chain acyl-CoA synthetase) and one HACD (very-long-chain (3R)-3-hydroxyacyl-CoA dehydratase), while up-regulated PSDs comprised an ALDH (acetaldehyde dehydrogenase), an ADH (alcohol dehydrogenase), two LOX2Ss (lipoxygenase) and one HPL (hydroperoxide lyase) (Fig. 3b). To validate the function of key genes (the two ACSLs, the ALDH and the ADH) in decanal biosynthesis, we produced the recombinant proteins of these genes and conducted *in vitro* enzyme activity assay (see Methods). The final products of the *in vitro* reactions identified by LC–MS or GC–MS are consistent with the standards (Fig. 3 c-e). These results validate the enzyme activity of the two ASCLs in synthesizing hexadecanoyl-CoA as well as the ALDH and the ADH in synthesizing decanal and decanol.

To understand the transcriptional regulation of decanal biosynthesis, we conducted co-expression network analysis and found one module containing two key genes (*FpumACSL10* and *FpumALDH1*) and four potential regulating transcription factors (two *HD-ZIP*s, one *bHLH* and one *bZIP*) (Fig. 3f and Supplementary Table 13). Cis-element detection analysis revealed one G-box motif upstream of *FpumACSL10* and six G-box and one HD-Zip motifs upstream of *FpumALDH1* (Supplementary Table 14). As G-box binds to transcription factor families of bZIPs and bHLHs and HD-Zip binds to HD-ZIPs[35,36], we hypothesized that expression of *FpumACSL10* is regulated by the bHLH and the bZIP and all above four transcription

factors regulate the expression of *FpumALDH1*. To test this hypothesis, we obtained qualified polyclonal antibodies for the four transcription factors and performed ChIP-qPCR experiments. High % input and fold enrichment values showed that the bHLH and the bZIP could bind to the promoter region of *FpumACSL10* and all the four transcription factors could bind to the promoter region of *FpumALDH1* (Fig. 3g, h), providing evidence for our hypothesis.

Metabolic and genomic signature of antagonistic interaction

To understand the mechanisms of antagonistic interaction between figs of *F. pumila* var. *pumila* and larvae of *W. pumilae*, we analyzed chemical profiles of different tissue types of female and functional male figs at the receptive and the post-receptive stage using metabolomic data (Supplementary Table 7; see Methods). We focused on the secondary metabolites associated with plant chemical defenses (SMCDs)[22,37-39], comprising some terpenoids (triterpenes and sesquiterpenes) and phenylpropanoids (including their precursors and their derivatives) (Supplementary Fig. 12). Metabolomic analysis revealed 736 SMCDs (108 terpenoids and 628 phenylpropanoids) (Supplementary Table 15). While we found significant differences in chemical profiles between two types of tissues and between different fig development stages, there were few differences between female and functional male figs (Fig. 4a). No secondary metabolites with significant difference in quantity (SMSDs) were found between feeder and seed florets at the receptive stage, and there were only three SMSDs between galled ovules and seeds at the post-receptive stage

295 (Fig. 4b). Remarkably, we found similar changes of SMSDs in both the feeder floret-
296 galled ovule and the seed floret-seed transitions (Fig. 4c and Supplementary Fig. 13a).
297 Besides SMCDs, galled ovules and seeds shared similar overall chemical profiles
298 (Supplementary Fig. 14). These results showed similar chemical changes and profiles
299 in the development of female florets no matter they were parasitized by pollinator
300 larvae (becoming galled ovules) or not (developing into seeds).

301 As might be expected from organisms that spend most their lives in a specific
302 environment, contraction of three gene families crucial to the detoxification of plant
303 defensive chemicals[40] (CYP450s, glutathione s-transferases (GSTs) and
304 carboxylesterases (CCEs) gene families) was found in the genomes of *W. pumilae*, *E.*
305 *verticillata* and *C. solmsi* (Fig. 4d and Supplementary Fig. 15). Such contraction was
306 mainly caused by gene loss and infrequent tandem duplication (Supplementary Fig.
307 7b-d), and most of the detoxification-related genes in the three pollinating wasp
308 species were in the same monophyletic groups (Supplementary Fig. 16). Ten out of
309 the 56 detoxification-related genes in *W. pumilae* was at a high level (read counts >
310 200) and was significantly upregulated at the larval stage compared to the adult stage
311 (Supplementary Fig. 17 and Supplementary Table 16). These metabolic and genomic
312 signatures provide a molecular basis for further exploring the mechanisms of fig-
313 pollinator coadaptation during their antagonistic interaction.

314 **Discussion**

315 Reciprocal selection on signaling and defense traits has shaped the molecular
316 constraints governing how antagonistic larvae develop into mutualistic adult

317 pollinators[8,41]. In this study, our combination of classic electrophysiological
318 experiments and multi-omics approaches has illuminated some key mechanisms
319 forming the coadaptation in a pair of fig-pollinator mutualists. We identified the
320 attractive VOC, detected that host identification by the specific pollinators may be
321 linked to their reduced number of OBP genes, and validated an OBP mainly binding
322 the attractant. We identified the key genes involved in the regulation of both attractant
323 and repellent biosynthesis in the plant: from facilitating the synthesis of the repellent
324 to favoring the production of the attractant. Surprisingly, matched changes in SMCDs
325 occurred across the transitions from i) floret to galled ovule and ii) floret to seed, and
326 almost identical profiles of SMCDs were found in galled ovules and seeds. As for the
327 pollinator, we detected a contraction of detoxification-related gene families.
328 Previous studies have mainly focused on the dominant components or the
329 bouquet of components in the VOCs emitted by figs[14,17]. In contrast our results
330 showed that only one VOC of relative low concentration attracts the focal pollinating
331 wasp species, addressing the importance of detailing the complete spectrum of VOCs.
332 Moreover, the attractive VOC (an aldehyde) in our focal species is distinct from the
333 attractants found in other *Ficus* species (usually terpenes)[11,13,14,17,18]. Such a dramatic
334 difference indicates deep divergence among congeners in the recognition of VOC
335 attractants[42,43], providing the basis for adaptive radiations in both *Ficus* and their
336 pollinating wasps[44]. In addition, similar concentration of the attractant emitted by
337 different sexes of figs supports the intersexual mimicry hypothesis in *Ficus* species[21],
338 which argues that any changes in biosynthesis of attractant VOCs in female figs may

cause loss of sexual reproduction[21].

Similar chemical changes in the development of galled ovules and seeds and almost identical SMCD profiles in these tissues showed that the occupancy of pollinator larvae activates the reproductive program of galled ovules. This suggests that galling strategy may help pollinator larvae avoid the potential chemical sanctions when they exploit nutrients of host plants. This is likely to result from either pollinator larvae manipulating plant physiology or changes triggered by host figs once the feeder florets are galled. Chemical mimicry of fruits and seeds has been reported in other galling insects[24,25], while many studies also suggest that figs have evolved to accommodate pollinator larvae[10,15]. Other possibilities, such as pollination before oviposition combined with minimal initial interference of pollinator larvae can be largely excluded, because most galled ovules were not pollinated. Furthermore, we collected figs at the middle (four weeks after the entrance of pollinator foundresses) of the post-receptive stage (generally lasting 8-10 weeks). Future research should perform bioassays to determine the chemicals inducing the development of galled ovules and the specific secondary metabolites defending against pollinator larvae. This will reveal how pollinator larvae activate the reproductive programs of host plants and why they can only utilize feeder florets.

The pollinating wasp species have evolved specializations in OBP and detoxification-related genes, probably because they are host specific and spend most of their lives inside galled ovules (though some detoxification-related genes are not only involved in detoxification but also important for the general life cycle of insets).

Such specializations facilitate the maintenance of host-specificity, but conservation of some OBP genes among pollinating wasps (Supplementary Figs. 6, 7) may also offer opportunities for host shift[19,45,46]. Moreover, selection to maximize pollinator fitness may drive rapid adaptive changes in fig traits like floral scents, and such reciprocal selection has occurred in some generalized plant-pollinator systems[47].

Ongoing global changes are causing rapid evolution and phenotypic changes in many plants, leading to mismatches between key traits bridging plants and their pollinators[4,48]. Erosion of these links can result in the collapse of long-evolved mutualisms and a loss of biodiversity, but may also lead to the rewiring of host association networks[4,49,50]. Limitations to our knowledge of molecular determination in plant-pollinator interactions have made predictions about future changes in biodiversity and ecosystem functioning largely speculative. Our findings offer an example of gene for gene coadaptation that extends beyond the existing phenotype-based models of mutualism persistence[51] and place trait-based multi-omics at the center of the ecological and evolutionary research concerning interacting species in more diffuse systems.

References

1. Lamichhaney, S. et al. Evolution of Darwin's finches and their beaks revealed by genome sequencing. *Nature* **518**, 371–375 (2015).
2. Simões, M. et al. The evolving theory of evolutionary radiations. *Trends Ecol. Evol.* **31**, 27–34 (2016).
3. Arnegard, M. E. et al. Genetics of ecological divergence during speciation.

Nature **511**, 307–311 (2014).

4. Hoffmann, A. A. & Sgrò, C. M. Climate change and evolutionary adaptation. *Nature* **470**, 479–485 (2011).

5. Olsen, J. L. et al. The genome of the seagrass *Zostera marina* reveals angiosperm adaptation to the sea. *Nature* **530**, 331–335 (2016).

6. Becerra, J. X., Nogeb, K. & Venable, D. L. Macroevolutionary chemical escalation in an ancient plant–herbivore arms race. *Proc. Natl. Acad. Sci. USA* **106**, 18062–18066 (2009).

7. Edger, P. P. et al. The butterfly plant arms-race escalated by gene and genome duplications. *Proc. Natl. Acad. Sci. USA* **112**, 8362–8366 (2015).

8. Adler, L. S. & Bronstein, J. L. Attracting antagonists: does floral nectar increase leaf herbivory? *Ecology* **85**, 1519–1526 (2004).

9. McCall, A. C. & Irwin, R. E. Florivory: the intersection of pollination and herbivory. *Ecol. Lett.* **9**, 1351–1365 (2006).

10. Cook, J. M. & Rasplus, J.-Y. Mutualists with attitude: coevolving fig wasps and figs. *Trends Ecol. Evol.* **18**, 241–248 (2003).

11. Zhang, X. et al. Genomes of the banyan tree and pollinator wasp provide insights into fig-wasp coevolution. *Cell* **183**, 1–15 (2020).

12. Herre, E. A., Jandér, K. C. & Machado, C. A. Evolutionary ecology of figs and their associates: recent progress and outstanding puzzles. *Annu. Rev. Ecol. Evol. Syst.* **39**, 439–458 (2008).

13. Souza, C. D. et al. Diversity of fig glands is associated with nursery mutualism in

405 fig trees. *Am. J. Bot.* **102**, 1564–1577 (2015).
406 14. Souto-Vilarós, D. et al. Pollination along an elevational gradient mediated both by
407 floral scent and pollinator compatibility in the fig and fig-wasp mutualism. *J.*
408 *Ecol. Evol.* **106**, 2256–2273 (2018).
409 15. Wang, R. et al. Loss of top-down biotic interactions changes the relative benefits
410 for obligate mutualists. *Proc. R. Soc. B.* **286**, 20182501 (2019).
411 16. Mori K. et al. Identification of RAN1 orthologue associated with sex
412 determination through whole genome sequencing analysis in fig (*Ficus carica L.*).
413 *Sci. Rep.* **7**, 41124 (2017).
414 17. Proffit M. et al. Chemical signal is in the blend: bases of plant-pollinator
415 encounter in a highly specialized interaction. *Sci. Rep.* **10**, 10071 (2020).
416 18. Chen, C. et al. Private channel: a single unusual compound assures specific
417 pollinator attraction in *Ficus semicordata*. *Funct. Ecol.* **23**, 941–950 (2009).
418 19. Wang, G., Cannon, C. H. & Chen, J. Pollinator sharing and gene flow among
419 closely related sympatric dioecious fig taxa. *Proc. R. Soc. B.* **283**, 20152963
420 (2016).
421 20. Yu, H. et al. De novo transcriptome sequencing in *Ficus hirta* Vahl. (Moraceae) to
422 investigate gene regulation involved in the biosynthesis of pollinator attracting
423 volatiles. *Tree Genet. Genomes* **11**, 91 (2015).
424 21. Soler, C. C. L., Proffit, M., Bessière, J.-M., Hossaert -McKey, M. & Schatz, B.
425 Evidence for intersexual chemical mimicry in a dioicous plant. *Ecol. Lett.* **15**,
426 978–985 (2012).

22. Volf, M. et al. Community structure of insect herbivores is driven by conservatism, escalation and divergence of defensive traits in *Ficus*. *Ecol. Lett.* **21**, 83–92 (2018).
23. Martinson, E.O., Hackett, J.D., Machado, C.A. & Arnold A.E. Metatranscriptome analysis of fig flowers provides insights into potential mechanisms for mutualism stability and gall induction. *PLoS ONE* **10**, e0130745 (2015).
24. Zhang, H. et al. Leaf-mining by *Phyllonorycter blancardella* reprograms the host-leaf transcriptome to modulate phytohormones associated with nutrient mobilization and plant defense. *J. Insect Physiol.* **84**, 114–127 (2016).
25. Schultz, J.C., Edger, P.P., Body, M. & Appel, H.M. A galling insect activates plant reproductive programs during gall development. *Sci. Rep.* **9**, 1833 (2019).
26. The *Nasonia* Genome Working Group. Functional and evolutionary insights from the genomes of three parasitoid *Nasonia* species. *Science* **327**, 343–348 (2010).
27. Xiao, J.-H. et al. Obligate mutualism within a host drives the extreme specialization of a fig wasp genome. *Genome Biol.* **14**, R141 (2013).
28. Ohri, D. & Khoshoo, T. N. Nuclear DNA contents in the genus *Ficus* (Moraceae). *Plant Syst. Evol.* **156**, 1–4 (1987).
29. Chen, Y., Compton, S. G., Liu, M. & Chen, X.-Y. Fig trees at the northern limit of their range: the distributions of cryptic pollinators indicate multiple glacial refugia. *Mol. Ecol.* **21**, 1687–1701 (2012).
30. Chen, L.-G. et al. Binding affinity characterization of an antennae-enriched chemosensory protein from the white-backed planthopper, *Sogatella furcifera*

(Horváth), with host plant volatiles. *Pestic. Biochem. Phys.* **152**, 1–7 (2018).

31. Gu, S.-H. et al. Functional characterization and immunolocalization of odorant binding protein 1 in the lucerne plant bug, *Adelphocoris lineolatus* (GOEZE). *Arch. Insect Biochem.* **77**, 81–98 (2011).

32. Leal, W. S. et al. Reverse and conventional chemical ecology approaches for the development of oviposition attractants for *Culex* mosquitoes. *PLoS ONE* **3**, e3045 (2008).

33. Rizzo, W. B. et al. Fatty aldehyde and fatty alcohol metabolism: review and importance for epidermal structure and function. BBA-Mol. *Cell Biol. L.* **1841**, 377–389 (2014).

34. Schwab, W., Davidovich-Rikanati, R. & Lewinsohn, E. Biosynthesis of plant-derived flavor compounds. *Plant J.* **54**, 712–732 (2008).

35. Capella, M., Ribone, P. A., Arce, A. L. & Chan, R. L. *Arabidopsis thaliana* HomeoBox 1 (AtHB1), a Homedomain-Leucine Zipper I (HD-Zip I) transcription factor, is regulated by PHYTOCHROME-INTERACTING FACTOR 1 to promote hypocotyl elongation. *New Phytol.* **207**, 669–682 (2015).

36. Jiang, W. et al. Two transcription factors TaPpm1 and TaPpb1 co-regulate anthocyanin biosynthesis in purple pericarps of wheat. *J. Exp. Bot.* **69**, 2555–2567 (2018).

37. Guan, R. et al. Draft genome of the living fossil *Ginkgo biloba*. *GigaScience* **5**, 49 (2016).

38. Mithöfer, A., & Boland, W. Plant defense against herbivores: chemical aspects.

Annu. Rev. Plant Biol. **63**, 431–450 (2012).

39. Salazar, D. et al. Origin and maintenance of chemical diversity in a species-rich tropical tree lineage. *Nat. Ecol. Evol.* **2**, 983–990 (2018).
40. Després, L., David, J. P. & Gallet, C. The evolutionary ecology of insect resistance to plant chemicals. *Trends Ecol. Evol.* **22**, 298–307 (2007).
41. Segar, S. T., Volf, M., Sisol, M., Pardikes, N. & Souto-Vilarós, A. D. Chemical cues and genetic divergence in insects on plants: conceptual cross pollination between mutualistic and antagonistic systems. *Curr. Opin. Insect Sci.* **32**, 83–90 (2019).
42. Cook, J. M. & Segar, S. T. Speciation in fig wasps. *Ecol. Entomol.* **35**, 54–66 (2010).
43. Cruaud, A. et al. An extreme case of plant-insect codiversification: figs and fig-pollinating wasps. *Syst. Biol.* **61**, 1029–1047 (2012).
44. Yu, H. et al. Multiple parapatric pollinators have radiated across a continental fig tree displaying clinal genetic variation. *Mol. Ecol.* **28**, 2391–2405 (2019).
45. Satler, J. D. et al. Inferring processes of coevolutionary diversification in a community of Panamanian strangler figs and associated pollinating wasps. *Evolution* **73**, 2295–2311 (2019).
46. Wang, G. et al. Genomic evidence of prevalent hybridization throughout the evolutionary history of the fig-wasp pollination mutualism. *Nat. Commun.* **12**, 718 (2021).
47. Hoballah, M. E. et al. Single gene-mediated shift in pollinator attraction in

493 Petunia. *Plant Cell* **19**, 779–790 (2007).
494 48. Potts, S. G. et al. Global pollinator declines: trends, impacts and drivers. *Trends*
495 *Ecol. Evol.* **25**, 345–353 (2010).
496 49. Kiers, E. T., Palmer, T. M., Ives, A. R., Bruno, J. F. & Bronstein, J. L. Mutualisms
497 in a changing world: an evolutionary perspective. *Ecol. Lett.* **13**, 1459–1474
498 (2010).
499 50. Segar, S. T., Fayle, T .M., Srivastava, D. S., Lewinsohn, T. M., Lewis, O. T.,
500 Novotny, V., Kitching, R. L. & Maunsell, S. C. The role of evolution in shaping
501 ecological networks. *Trends Ecol. Evol.* **35**, 454-466 (2020).
502 51. Stoy, K. S., Gibson, A. K., Gerardo, N. M. & Morran, L. T. A need to consider the
503 evolutionary genetics of host-symbiont mutualisms. *J Evol. Biol.* **33**, 1656–1668
504 (2020).
505 52. Marçais, G. & Kingsford, C. A fast, lock-free approach for efficient parallel
506 counting of occurrences of k-mers. *Bioinformatics* **27**, 764–770 (2011).
507 53. Xiao, C.-L. et al. MECAT: fast mapping, error correction, and de novo assembly
508 for single-molecule sequencing reads. *Nat. Methods* **14**, 1072–1074 (2017).
509 54. Walker, B. J. et al. Pilon: an integrated tool for comprehensive microbial variant
510 detection and genome assembly improvement. *PLoS One* **9**, e112963 (2014).
511 55. Pryszcz, L. P., & Gabaldón, T. Redundans: an assembly pipeline for highly
512 heterozygous genomes. *Nucleic Acids Res.* **44**, e113 (2016).
513 56. Zhang, Z., Schwartz, S., Wagner, L. & Miller, W. A greedy algorithm for aligning
514 DNA sequences. *J. Comput. Biol.* **7**, 203–214 (2000).

515 57. English, A. C. et al. Mind the gap: upgrading genomes with Pacific Biosciences
516 RS long-read sequencing technology. *PLoS ONE* **7**, e47768 (2012).
517 58. Sahlin, K., Chikhi, & Arvestad, R. L. Assembly scaffolding with PE-
518 contaminated mate-pair libraries. *Bioinformatics* **32**, 1925–1932 (2016).
519 59. Belton, J. M. et al. Hi-C: a comprehensive technique to capture the conformation
520 of genomes. *Methods* **58**, 268–276 (2012).
521 60. Servant, N. et al. (2015) HiC-Pro: an optimized and flexible pipeline for Hi-C
522 data processing. *Genome Biol.* **16**, 259.
523 61. Durand, N.C. et al. Juicer provides a one-click system for analyzing loop-
524 resolution Hi-C experiments. *Cell Syst.* **3**, 95–98 (2016).
525 62. Dudchenko, O. et al. De novo assembly of the Aedes aegypti genome using Hi-C
526 yields chromosome-length scaffolds. *Science* **356**, 92–95 (2017).
527 63. Simão, F. A., Waterhouse, R. M., Ioannidis, P., Kriventseva, E. V. & Zdobnov, E.
528 M. BUSCO: assessing genome assembly and annotation completeness with
529 single-copy orthologs. *Bioinformatics* **31**, 3210–3212 (2015).
530 64. Wu, T. D. & Watanabe, C. K. GMAP: a genomic mapping and alignment program
531 for mRNA and EST sequences. *Bioinformatics* **21**, 1859–1875 (2005).
532 65. Benson, G. Tandem repeats finder: a program to analyze DNA sequences. *Nucleic*
533 *Acids Res.* **27**, 573–580 (1999).
534 66. Bao, W., Kojima, K. K. & Kohany, O. Repbase Update, a database of repetitive
535 elements in eukaryotic genomes. *Mobile DNA* **6**, 11 (2015).
536 67. Xu, Z. & Wang, H. LTR_FINDER: an efficient tool for the prediction of full-

length LTR retrotransposons. *Nucleic Acids Res.* **35**, W265–W268 (2007).

68. Edgar, R. C. & Myers, E. W. PILER: identification and classification of genomic repeats. *Bioinformatics* **21**, i152–i158 (2005).

69. Price, A. L., Jones, N. C. & Pevzner, P. A. De novo identification of repeat families in large genomes. *Bioinformatics* **21**, i351–i358 (2005).

70. Lowe, T. M. & Eddy, S. R. tRNAscan-SE: a program for improved detection of transfer RNA genes in genomic sequence. *Nucleic Acids Res.* **25**, 955–964 (1997).

71. Nawrocki, E. P. & Eddy, S. R. Infernal 1.1: 100-fold faster RNA homology searches. *Bioinformatics* **29**, 2933–2935 (2013).

72. Nawrocki, E.P. et al. Rfam 12.0: updates to the RNA families database. *Nucleic Acids Res.* **43**, D130–D137 (2015).

73. Holt, C. & Yandell, M. MAKER2: an annotation pipeline and genome-database management tool for second-generation genome projects. *BMC Bioinformatics* **12**, 491 (2011).

74. Kim, D., Langmead, B. & Salzberg, S.L. HISAT: a fast spliced aligner with low memory requirements. *Nat. Methods* **12**, 357–360 (2015).

75. Pertea, M. et al. StringTie enables improved reconstruction of a transcriptome from RNA-seq reads. *Nat. Biotechnol.* **33**, 290–295 (2015).

76. Johnson, A. D. et al. SNAP: a web-based tool for identification and annotation of proxy SNPs using HapMap. *Bioinformatics* **24**, 2938–2939 (2008).

77. Stanke, M. & Morgenstern, B. AUGUSTUS: a web server for gene prediction in

559 eukaryotes that allows user-defined constraints. *Nucleic Acids Res.* **33**, W465–
560 W467 (2005).
561 78. Buels, R. et al. JBrowse: a dynamic web platform for genome visualization and
562 analysis. *Genome Biol.* **17**, 66 (2016).
563 79. Buchfink, B., Xie, C. & Huson, D.H. Fast and sensitive protein alignment using
564 DIAMOND. *Nat. Methods* **12**, 59–60 (2015).
565 80. Bairoch, A. & Apweiler, R. The SWISS-PROT protein sequence database and its
566 supplement TrEMBL in 2000. *Nucleic Acids Res.* **28**, 45–48 (2000).
567 81. Kanehisa, M., Sato, Y., Kawashima, M., Furumichi, M. & Tanabe, M. KEGG as a
568 reference resource for gene and protein annotation. *Nucleic Acids Res.* **44**, D457–
569 D462 (2016).
570 82. Jones, P. et al. InterProScan 5: genome-scale protein function classification.
571 *Bioinformatics* **30**, 1236–1240 (2014).
572 83. Conesa, A. et al. Blast2GO: a universal tool for annotation, visualization and
573 analysis in functional genomics research. *Bioinformatics* **21**, 3674–3676 (2005).
574 84. Li, L., Stoeckert, C. J., Jr. & Roos, D. S. OrthoMCL: identification of ortholog
575 groups for eukaryotic genomes. *Genome Res.* **13**, 2178–2189 (2003).
576 85. Li, H. et al. TreeFam: a curated database of phylogenetic trees of animal gene
577 families. *Nucleic Acids Res.* **34**, D572–D580 (2006).
578 86. Edgar, R. C. MUSCLE: multiple sequence alignment with high accuracy and high
579 throughput. *Nucleic Acids Res.* **32**, 1792–1797 (2004).
580 87. Capella-Gutierrez, S., Silla-Martinez, J.M. & Gabaldon, T. trimAl: a tool for

automated alignment trimming in large-scale phylogenetic analyses. *Bioinformatics* **25**, 1972–1973 (2009).

88. Guindon, S., Delsuc, F., Dufayard, J. F. & Gascuel, O. Gascuel, Estimating maximum likelihood phylogenies with PhyML. *Methods Mol. Biol.* **537**, 113–137 (2009).
89. Yang, Z. PAML 4: phylogenetic analysis by maximum likelihood. *Mol. Biol. Evol.* **24**, 1586–1591 (2007).
90. De Bie, T., Cristianini, N., Demuth, J. P. & Hahn, M. W. CAFE: a computational tool for the study of gene family evolution. *Bioinformatics* **22**, 1269–1271 (2006).
91. Tang, H. et al. Unraveling ancient hexaploidy through multiply-aligned angiosperm gene maps. *Genome Res.* **18**, 1944–1954 (2008).
92. Schwartz, S. et al. Human-mouse alignments with BLASTZ. *Genome Res.* **13**, 103–107 (2003).
93. Bailey, J. A., Yavor, A. M., Massa, H. F., Trask, B. J. & Eichler, E. E. Segmental duplications: organization and impact within the current human genome project assembly. *Genome Res.* **11**, 1005–1017 (2001).
94. Birney, E., Clamp, M. & Durbin, R. GeneWise and Genomewise. *Genome Res.* **14**, 988–995 (2004).
95. Ruan, J., Li, H., Chen, Z. & Coghlan, A. TreeFam: 2008 Update. *Nucleic Acids Res.* **36**, D735–D740 (2008).
96. Tholl, D. et al. Practical approaches to plant volatile analysis. *Plant J.* **45**, 540–560 (2006).

603 97. Wen, B., Mei, Z., Zeng, C. & Liu, S. metaX: a flexible and comprehensive
604 software for processing metabolomics data. *BMC Bioinformatics* **18**, 183 (2017).
605 98. Wen, P. et al. The sex pheromone of a globally invasive honey bee predator, the
606 Asian eusocial hornet, *Vespa velutina*. *Sci. Rep.* **7**, 12956 (2017).
607 99. Chen, Y., Chen, Y., Shi, C. & Huang, Z. et al. SOAPnuke: a MapReduce
608 acceleration-supported software for integrated quality control and preprocessing
609 of high-throughput sequencing data. *Gigascience* **7**, 1–6 (2018).
610 100. Langmead, B. & Salzberg, S. L. Fast gapped-read alignment with Bowtie 2. *Nat.*
611 *Methods* **9**, 357–359 (2012).
612 101. Li, B. & Dewey, C. N. RSEM: accurate transcript quantification from RNA-Seq
613 data with or without a reference genome. *BMC Bioinformatics* **12**, 323 (2011).
614 102. Tian, X., Chen, L., Wang, J., Qiao, J. & Zhang, W. Quantitative proteomics
615 reveals dynamic responses of Synechocystis sp. PCC 6803 to next-generation
616 biofuel butanol. *J. Proteomics* **78**, 326–345 (2013).
617 103. Wen, B., Zhou, R., Feng, Q., Wang, Q., Wang, J. & Liu, S. IQuant: an automated
618 pipeline for quantitative proteomics based upon isobaric tags. *Proteomics* **14**,
619 2280–2285 (2014).
620 104. Brosch, M., Yu, L., Hubbard, T. & Choudhary, J. Accurate and sensitive peptide
621 identification with Mascot Percolator. J. *Proteome Res.* **8**, 3176–3181 (2009).
622 105. Savitski, M. M., Wilhelm, M., Hahne, H., Kuster, B. & Bantscheff, M. A scalable
623 approach for protein false discovery rate estimation in large proteomic data sets.
624 *Mol. Cell. Proteomics* **14**, 2394–2404 (2015).

106. Cox, J. & Mann, M. MaxQuant enables high peptide identification rates, individualized p.p.b.-range mass accuracies and proteome-wide protein quantification. *Nat. Biotechnol.* **26**, 1367–1372 (2008).

107. Bruderer, R. et al. Extending the limits of quantitative proteome profiling with data-independent acquisition and application to acetaminophen-treated three-dimensional liver microtissues. *Mol. Cell. Proteomics* **14**, 1400–1410 (2015).

108. Dunn, W.B. et al. Procedures for large-scale metabolic profiling of serum and plasma using gas chromatography and liquid chromatography coupled to mass spectrometry. *Nat. Protoc.* **6**, 1060–1083 (2011).

109. Love, M. I., Huber, W. & Anders, S. Moderated estimation of fold change and dispersion for RNA-seq data with DESeq2. *Genome Biol.* **15**, 550 (2014).

110. Choi, M. et al. MSstats: an R package for statistical analysis of quantitative mass spectrometry-based proteomic experiments. *Bioinformatics* **30**, 2524–2526 (2014).

111. Wen, X.-L., Wen, P., Dahlsjö, C. A. L., Sillam-Dussès, D. & Šobotník, J. Breaking the cipher: ant eavesdropping on the variational trail pheromone of its termite prey. *Proc. R. Soc. B.* **284**, 20170121 (2017).

112. Bailey, T. L. & Elkan, C. Fitting a mixture model by expectation maximization to discover motifs in biopolymers. *Proc. Int. Conf. Intell. Syst. Mol. Biol.* **2**, 28–36 (1994).

113. Langfelder, P. & Horvath, S. WGCNA: an R package for weighted correlation network analysis. *BMC Bioinformatics* **9**, 559 (2008).

114. Yip, A. M. & Horvath, S. Gene network interconnectedness and the generalized topological overlap measure. *BMC Bioinformatics* **8**, 22 (2007).

115. Langfelder, P., Zhang, B. & Horvath, S. Defining clusters from a hierarchical cluster tree: the dynamic tree cut package for R. *Bioinformatics* **24**, 719–720 (2008).

116. Lescot, M. et al. PlantCARE, a database of plant cis-acting regulatory elements and a portal to tools for in silico analysis of promoter sequences. *Nucleic Acids Res.* **30**, 325–327 (2002).

117. Gendrel, A.V., Lippman, Z., Martienssen, R. & Colot V. Profiling histone modification patterns in plants using genomic tiling microarrays. *Nat. Methods* **2**, 213–218 (2005).

ACKNOWLEDGMENTS

We thank Yong-Jin Wang, Qi-Chong Zhu, Qiong Sun, Qian-Ya Li, Jing-Wen Wang, Tong-Lei Xu, Yue Chen, Fang-Lu Wei, Guo-Chun Shen, Xiu-Lian Wen and Li-Sha Li for their kind helps in field experiments, Xiu-Lian Wen, Li-Sha Li and the Public Technology Service Center of XTBG (CAS) for assisting active VOCs analysis, and Xiu-Guang Mao, Pan-Yu Hua and Da-Yong Zhang for constructive suggestions in data analysis. This work is supported by NSFC grants 31630008 and 31870356 (X.-Y.C.), and 31870359 (G.W.); and a Talents 1000 Fellowship of Shaanxi Province (D.W. D.). S.S. acknowledges departmental support from Harper Adams University.

Author contributions

X.-Y.C. and R.W. conceived and designed the study. R.W., Y.Yang., S.G.C., S.T.S., H.Y. and Z.Y. conducted the experiments and analyzed data. Y.J., Q.-F.L., H.Y., Y.Z., G.W., J.C., R.M., S.C., Y.C., D.W.D., H.-Q.L., M.L., Y.-Y.D., Y.-Y.L., X.T., P.W., J.-J.Y., X.-T.Z., Q.G., J.-Y.Y., Y.Yin, K.J. and H.-M.Y. contributed to data acquisition and data analyses. R.W., S.S., S.G.C., J.-Q.L., J.-Y.R., F.K., C.A.M, A.C., P.M.G, Y.-Y.Z. and X.-Y.C. edited the manuscript. All authors contributed to writing the manuscript.

Competing interests

The authors declare no competing interests.

Additional information

All supplemental figures and tables are included in supplementary information.

Figure legends

Fig. 1 | Fig-pollinator mutualism between *F. pumila* var. *pumila* and *Wiebesia pumilae* and determination of the compound attracting *W. pumilae*. a, Life cycle of *W. pumilae* based on four fig developmental stages (pre-receptive, receptive, post-receptive and mature stages). This *Ficus* species is dioecious with figs on female trees growing long-styled female florets (seed florets) that are not available for pollinator oviposition. Therefore, female trees only produce seeds, while figs on functional male

691 trees contain both male florets and short-styled female florets (feeder florets) that can
692 be used by female pollinators for oviposition to support the larvae of the pollinators.
693 At the receptive stage, adult female pollinators are attracted by host-specific VOCs
694 and enter figs only through ostiole (lined with bracts), either ovipositing into ovules of
695 feeder florets in functional male figs or pollinating seed florets inside female figs.
696 Pollinator larvae develop in induced galled ovules and both larvae and seeds grow
697 during the post-receptive stage. At the mature stage, after mating with adult males,
698 adult female pollinators leave their natal figs carrying pollen donated by mature male
699 florets and search for receptive figs and complete the cycle. **b,** Electrophysiological
700 responses of adult females of *W. pumilae* to the VOCs extracted from *F. pumila* var.
701 *pumila* figs at receptive stage using GC–EAD. Each curve represents the response of a
702 single female pollinator. **c,** Electrophysiological responses of adult female pollinators
703 to the synthesized standard of each tentative VOC compound (each
704 electroantennogram curve represents five overlapped replicates). **d,** Preference of
705 adult female pollinators to different tentative compounds using Y-tube olfactometer
706 tests (Supplementary Table 9).
707
708 **Fig. 2 | Molecular mechanisms of the specific host identification of *W. pumilae*. a,**
709 Numbers of genes in the four olfactory-related gene families (odorant-binding
710 proteins (OBPs), olfactory receptors (ORs), chemosensory proteins (CSPs) and
711 ionotropic receptor (IRs)) in different insect species. Significantly contracted families
712 (***: $p<0.001$) were shown for *W. pumilae* and *C. solmsi*, and species were ranked

according to their phylogeny (Supplementary Fig. 4b). **b,** Transcription and translation of OBP genes of adult females of *W. pumilae* not contacting (as the control) and contacting the VOCs emitted by *F. pumila* var. *pumila* figs at the receptive stage (Supplementary Table 10). **c,** Motif analysis predicting the most likely *W. pumilae* OBPs that can bind to decanal and nonanal (Supplementary Fig. 9). **d,** The binding affinities (K_D) of the predicted OBPs to decanal and nonanal using surface plasmon resonance (SPR) experiments (Supplementary Fig. 10 and Supplementary Table 11). Lower K_D indicates higher binding affinity, and error bars represent standard errors calculated by parameter estimation in steady state affinity model.

Fig. 3 | Regulation of gene expression in attractant biosynthesis in figs of *F. pumila* var. *pumila*. a, Pathways associated with biosynthesis of decanal and nonanal (fatty acid biosynthesis (ko00061), elongation (ko00062) and metabolism (ko00071 and ko00592)). **b,** Fold changes of all PSDs and their transcriptomic expression between receptive and pre-receptive stages in ostiolar types in proteomes (Supplementary Table 12). ^{NS}: $p>0.05$, *: $p<0.05$, **: $p<0.01$, ***: $p<0.001$. **c-e,** Results of *in vitro* functional characterization of the four key genes in the biosynthesis of decanal and nonanal. The peaks of synthesized standards and reaction products (treatments with enzyme added for three replicates) were shown for each key gene. Because there are two steps in the catalytic reaction of the two ACSLs, we showed the ion intensity of both the intermediate product (hexadecanoyl-AMP) and the final product (hexadecanoyl-CoA) separated by LC–MS. The reaction products of the

735 ALDH and the ADH (decanal and decanol) were identified using GC–MS. **f,**
736 Transcriptomic expression of genes in the co-expression module including two key
737 genes and the transcription factors predicted to regulate the expression of these two
738 key genes (Supplementary Tables 13 and 14). **g-h,** Results of ChIP–qPCRs (% input
739 and fold enrichment) showing the evidence that the predicted transcription factors can
740 bind to the promoter regions of *FpumACSL10* (FPUM_023966-RA) and
741 *FpumALDH1* (see Supplementary Tables 12 and 13). Error bars represent standard
742 errors of experimental results.
743
744 **Fig. 4 | Metabolic and genomic signature of antagonistic interaction between *F.***
745 ***pumila* var. *pumila* and *W. pumilae*. a,** Results of PLS-DA for terpenoids (triterpenes
746 and sesquiterpenes) and phenylpropanoids. Each oval indicates the 95% confidence
747 intervals of a sample group. **b,** Distribution of SMCDs across fates of female florets.
748 No SMSDs between feeder and seed florets and only three SMSDs (two
749 downregulated and one upregulated) between galled ovules and seeds were found in
750 the pathways related to plant chemical defenses (Supplementary Fig. 12). **c**, Largely
751 matched turnover of SMSDs in feeder floret-galled ovule and seed floret-seed
752 transitions (using Spearman's rank correlation tests). **d**, Numbers of genes in
753 CYP450, CCE and GST gene families in different insect species. Significantly
754 contracted families (***: $p<0.001$) were shown for *W. pumilae* and *C. solmsi*.

Table 1 | Summary statistics for the assembly of *F. pumila var. pumila* and *W. pumilae* genomes.

Chromosome ID	*F. pumila var. pumila*		*W. pumilae*	
	No. of genes	Length (bp)	No. of genes	Length (bp)
Chr1	1,697	20,463,500	816	21,315,831
Chr2	1,871	21,202,951	2,076	59,985,216
Chr3	2,335	23,199,346	2,631	66,440,284
Chr4	2,412	23,721,380	2,225	54,409,331
Chr5	3,327	31,603,922	2,281	59,419,729
Chr6	1,649	20,816,579	2,263	55,968,755
Chr7	2,070	23,331,000		
Chr8	2,097	21,006,959		
Chr9	1,856	21,788,500		
Chr10	1,740	20,107,953		
Chr11	1,798	22,360,920		
Chr12	2,000	20,847,995		
Chr13	2,526	34,592,857		
Number of contigs	543		102	
Total length of contigs (Mb)	315.7		318.2	
Contig N50 (Mb)	2.3		10.9	
Anchored genome content (Mb)	304.8		317.5	
Anchored rate	96.6%		99.8%	
Scaffold N50 (Mb)	22.4		59.4	
Number of genes	28,187		12,316	

Methods

Genome assembly and annotation. Genomic DNA was extracted from leaves of a female *F. pumila* var. *pumila* individual nearby Zhejiang Tiantong Forest Ecosystem National Observation and Research Station (TINAS) (E 121°47', N 29°48'), Ningbo, China, and from c. 500 adult female pollinators of *W. pumilae* emerged from five figs on a functional male tree in South China Botanic Garden (SCBG) (E 113°11', N 23°11'), Guangzhou, China. Six pair-end and mate-pair libraries were prepared with varying insert sizes (Supplementary Table 1) for sequencing on an Illumina Hiseq 4000 platform. We also carried out PacBio single-molecule real-time sequencing of 20kb SMRTbell libraries using a PacBio Sequel platform. Based on the Illumina pair-end sequencing data, the genome sizes of both species were estimated by counting k-mer frequency using Jellyfish version 2.1.3[52].

De novo genome assembly was conducted using MECAT version 1.2[53]. The initial contig was polished twice based on raw PacBio data and then corrected twice using Illumina paired-end reads with pilon version 1.22[54]. Redundans version 0.13c[55] was used to exclude redundant contigs, and we removed contaminative sequences by searching against the NCBI nucleotide sequences database (ftp://ftp.ncbi.nlm.nih.gov/blast/db/ FASTA/) using megablast[56] with e-value ≤ $1e^{-5}$. Gap filling was implemented with PBJelly[57] after scaffolding based on Illumina mate-pair reads using BESST version 2.2.7[58].

To further improve the quality of genome assembly of both species, we used high-throughput chromatin conformation capture (Hi-C) technique to scaffold contigs into pseudo-chromosomes. We constructed Hi-C libraries using the protocol described

782 by Belton et al.[59]. Fresh leaves sampled from the same *F. pumila* var. *pumila*
783 individual used in above sequencing and adult female pollinators from SCBG were
784 cross-linked by 4% formaldehyde solution, followed by an overnight digestion with a
785 4-cutter restriction enzyme MboI (400 units) at 37°C, preparation DNA ends with
786 biotin-14-dCTP and blunt-end ligation of the cross-linked fragments. Then, the
787 proximal chromatin DNA was re-ligated by ligation enzyme, and the nuclear
788 complexes were reverse cross-linked by proteinase K. After that, we extracted and
789 purified DNA and removed biotin from non-ligated fragment ends using T4 DNA
790 polymerase. The following steps including end reparation, enrichment of biotin-
791 labeled Hi-C samples, and ligation by Illumina paired-end (PE) sequencing adapters,
792 and then the Hi-C library (insert size of 350 bp) was amplified by PCR and sequenced
793 on an Illumina NovaSeq 6000 platform. High quality data checked by HiC-Pro[60] were
794 mapped to genome using BWA, with extraction of uniquely mapped reads for pseudo-
795 chromosome clustering and assembly using Juicer[61] and 3D-DNA[62].
796 Following genome assembly, we assessed completeness using BUSCO version
797 3.0.3[63] and Iso-Seq full-length transcripts. The high-quality full-length transcripts
798 were mapped to genome assemblies using GMAP version 2014-12-21[64], setting a
799 cutoff of aligned coverage at 0.85 and aligned identity at 0.9. The quality of genome
800 assembly was further tested by mapping Illumina paired-end reads to the genome
801 assemblies using BWA with the depth of coverage calculated using BamDeal version
802 0.19 (https://github.com/BGI-shenzhen/BamDeal/). For each species, Iso-Seq
803 sequencing was performed using a PacBio Sequel platform, based on two SMRTbell

libraries with insert sizes of 0 - 5kb and 4.5kb - 10kb established by full-length complementary DNA (cDNA). We used fresh leaves, young stems from fertile and sterile branchlets and figs at different developmental stages for the plant, and adult males and females for the pollinator.

Genome annotation includes repeat identification (including tandem repeats (TRs) and transposable elements (TEs)), annotation of non-coding RNAs (ncRNA) and gene prediction and annotation. When annotating repeat sequences, TRs were identified using Tandem Repeats Finder (TRF) version 4.07[65], and TEs were searched against Repbase 21.01[66] and the transposable element protein database using RepeatMasker version 4.0.6 (http://www.repeatmasker.org/) and RepeatProteinMask in RepeatMasker. LTR_Finder[67], PILER[68] and RepeatScout[69] were used to create a *de novo* TE library, and the combined non-redundant library was classified by running RepeatMasker again.

To annotate ncRNAs, tRNAscan-SE version 1.3.1[70] was used to identify tRNA and their secondary structures. While small nuclear RNA (snRNA) and microRNAs (miRNAs) were searched for using INFERNAL version 1.1.1[71] in the Rfam database version 12.0[72], followed by the detection of rRNAs by aligning with plant or invertebrate rRNA sequences using BLASTN (E-value $\leq 1e^{-5}$).

Gene model prediction was conducted using the MAKER pipeline version 2.31.10[73]. The Iso-Seq full-length transcripts, RNA-seq transcripts (assembled using Hisat2 version 2.0.1[74] and StringTie version 1.3.3[75]), the protein sequences of related species and protein sequences from Swiss-Prot database (https://www.uniprot.org)

were included in the analysis. Ab-initio gene prediction was performed with the gene predictors SNAP[76] and AUGUSTUS[77]. The MAKER pipeline was run for two (for the plant) and three (for the pollinator) iterations for training and the final trained hidden Markov model (HMM) was used for annotation. JBrowse version 1.12.3[78] was used to examine the gene models following each iteration. The gene models with the presence of a PFAM domain or with AED ≤ 0.6 for *W. pumilae* and AED＜1 for *F. pumila* var. *pumila* were retained. BUSCO was used to evaluate the completeness of gene annotation for both genomes.

After determining gene models, functions of protein-coding genes were annotated using DIAMOND version 0.8.23[79] by aligning them to NCBI NR database, Swiss-Prot[80] and KEGG[81] databases. Motifs and domains in protein sequences were annotated using InterProScan version 5.16-55.0[82] via searching public databases. Gene Ontology terms for each gene were assigned using Blast2GO version 3.3[83].

Comparative genomics. To analyze the evolutionary characters of our studied genomes, we first carried out gene family clustering. The genome and annotation data of 13 other angiosperm species and 11 other arthropod species were downloaded (Supplementary Table 6). The gene models with open reading frames shorter than 90bp were removed, and only the longest transcript was chosen to represent each gene. Gene family clustering was performed using OrthoMCL version 10-148[84] for the plant and TreeFam pipeline version 0.5.1[85] for the pollinator.

We then determined the phylogenetic relationships among the plants and among the insects in the species pools used in gene family clustering. Corresponding coding

sequences (CDSs) were aligned based on the protein sequences of all single-copy orthologs using MUSCLE version 3.8.31[86], and codon position 2 of aligned CDSs were concatenated into a super gene using an in-house Perl script with a filtration of ambiguously aligned positions using trimAI version 1.4.1[87]. After that, phylogenetic trees were reconstructed using PhyML version 3.0[88] using a GTR substitution model with a gamma distribution and 100 bootstrap replicates. PAML version 4.9[89] was used to estimate divergence time, setting 10,000 MCMC generations with a sampling frequency of 5,000 and a burn-in of 5,000,000 iterations. Overall substitution rate was assessed using BASEML setting a REV substitution model.

Gene family expansion and contraction was analyzed using CAFE version 2.1[90], which employed a stochastic birth-and-death process to model the evolution of gene family sizes over a phylogeny. The birth-and-death parameter (λ) was estimated using 10,000 Monte Carlo random samples. We then used family-wise method to statistically test if a gene family experienced significant expansion/contraction, and gene families with conditional P-values less than 0.05 were considered to have accelerated rates of gains and losses.

We then tested whether the genomes of *F. pumila* var. *pumila* experienced whole genome duplication (WGD). Syntenic blocks were identified using MCscan version 0.8[91], and the rate of transversions on fourfold degenerate synonymous sites (4DTv) was calculated using the HKY substitution model to uncover potential speciation or WGD events occurring in evolutionary history of the plant. For *W. pumilae*, we tested for genomic segmental duplications (SDs). The self-alignment was performed using

BLASTZ version 1.02[92], and a non-redundant set of SDs was obtained using WGAC version 1.3[93].

Annotation of specific gene families and analysis of their evolution. To test whether the contraction specific gene families in *W. pumilae*, *E. verticillata* and *C. solmsi* contributes to the wasps' host-specificity and detoxification ability, we conducted a detailed annotation in chemosensory gene families (OBPs, CSPs, ORs and IRs) and detoxification gene families including CYP450s, GSTs and CCEs. The homologous genes of *N. vitripennis*, *Apis mellifera* and *Drosophila melanogaster* were used as queries to search the genome assembly of *W. pumilae* using TBLASTN at a criterion of E-value $\leq 1e^{-5}$, and gene structures of identified genes were predicted using GeneWise version 2.4.1[94] with pseudogenes masked. We repeated this process iteratively until no more genes were detected. Additional genes from the MAKER annotation were also included if they included corresponding InterPro domains. All gene structures were manually checked and corrected if necessary, on the basis of full-length transcripts, RNA-seq transcripts and homologous proteins in JBrowse. We used Binomial Distribution One-tailed test to examine gene family expansion/contraction among the compared species without considering their evolutionary relationships.

To reveal the evolutionary history of OBP, CYP450, CCE and GST gene families, syntenic blocks were identified across the genomes of the three pollinating wasp species and *N. vitripennis* using MCscan (https://github.com/tanghaibao/jcvi/wiki/MCscan-(Python-version)). We then constructed neighbor-joining phylogenetic trees to verify homologous genes among these insect species, using TreeBeST version

892 1.9.2[95] using a JTT model and 1000 bootstraps.

893 **VOC collection and component analysis.** To reveal the composition of volatile
894 organic compounds (VOCs) emitted by figs of *F. pumila* var. *pumila* at different
895 developmental stages, we collected VOCs from figs at both pre-receptive and
896 receptive stages (Fig. 1a) in spring 2018 using dynamic headspace sampling (DHS)
897 techniques[96]. After a careful search, we chose ten mature *F. pumila* var. *pumila* trees
898 comprising five females and five functional males (Supplementary Table 8) nearby
899 TINAS, within the natural range of the plant. Three figs were labeled on each selected
900 individual. At either fig developmental stage (from early to middle April for pre-
901 receptive stage and late April for receptive stage), we extracted the VOCs emitted by
902 each labeled fig into an activated porapak adsorption tube (150 mg) during 8:00-11:00
903 am, using a protocol identical to Tholl et al. (2006)[96]. Each adsorption tube was then
904 eluted three times using 300 μl n-hexane and stored at -20 ℃.

905 VOCs emitted by figs were then separated and identified using a coupled Gas
906 Chromatography-Mass Spectrometry (GC–MS) system (HP 7890A-5975C, Agilent,
907 US)[97]. For each sample, 1.8 μl of eluate VOC extract, concentrated using nitrogen,
908 was injected in split mode with a split ratio of 10 : 1 at 250 ℃. Helium (1 mL/min)
909 was used as carrier gas in a HP-5ms (30 m × 250 μm × 0.25 μm, Agilent, US) GC
910 column. We set the oven ramp at 40℃ for 1 min, and then 3 ℃/min to 140 ℃ for 1
911 min, followed by 5 ℃/min to 230 ℃ for 3 mins. Ionization was conducted by
912 electron impact (70 eV, source temperature 230 ℃). The MS quadrupole was heated
913 to 150 ℃, with the scanned mass range setting as from 40 to 550 m/z. Compound

identification was implemented by matching the mass spectra with NIST 08 MS libraries. We then calculated the relative proportions of all compounds emitted by figs at each developmental stage.

To evaluate the difference in the concentration of decanal between ostiolar tissues and female florets, we sampled figs at receptive stages from three female and three functional male individuals and identified the composition of VOCs emitted from these two types of tissues using the same approach mentioned above. The decanal concentration in each type of tissues in a plant individual was quantified by comparing its peak area with the internal standard (decyl acetate).

Electrophysiological responses of pollinating wasps. To narrow the range of candidate VOCs attracting *W. pumilae*, we tested the electrophysiological responses of the pollinators to the collected VOCs, using gas chromatography-electroantennogram detection (GC–EAD). We used a system coupling a custom-made EAG[98] with a GC (Trace GC 2000, Themo Finnigan, US). We injected 1.8 μl of concentrated VOC extract eluate into the GC to separate different compounds. The GC conditions were identical to those used for the GC–MS component analysis, except that the oven ramp was set to 50 °C for 2 mins, and then to 10 °C/min up to 280 °C for 1 min. After GC–FID (flame ionization detector) quantification, outflow from the GC column was delivered to the EAG as the stimulus through a custom, 40 cm long heated (at 250 °C) transfer line with a clean, wet, and static-free airflow. The stimulus was then puffed to the antenna of an adult female pollinator (collected from figs in TINAS) fixed onto the EAG with both ends of the antennae connected with prepared glass electrodes

936 linking the probes of EAG to the potentiometric amplifiers.

937 This experiment was repeated 5 times (i.e. antennae of 5 adult female
938 pollinators), and the EAD signal was recorded using a HP 34465A digital multimeter
939 (Keysight, US). Both EAD and FID signal data were aligned to verify the tentative
940 compounds stimulating the adult female pollinator, using the software IO Libraries
941 Suite 16 (Agilent, US) and BenchVue (Keysight, US). These tentative effective
942 compounds were identified by matching the chromatographs with the results of
943 component analysis using GC–MS.

944 We further tested the electrophysiological response of adult female pollinators
945 (collected from figs in SCBG) to the synthesized standard of each tentative compound
946 (TIC, JPN; TRC, CAN; Sigma-Aldrich, US), following the same procedures as above.
947 A compound was determined as truly effective only when it was confirmed by the
948 experiments using both eluate of VOC extracts and synthesized standard.

949 **Behavioral preference of pollinating wasps.** To test the behavioral preference of *W.*
950 *pumilae* to different tentative effective VOCs, we used a Y-tube olfactometer (stem 8
951 cm, arms 9 cm, at an angle of 55°, internal diameter of 1.5 cm) following the methods
952 described by Wang et al.[19]. We placed the synthesized standard of each tentative
953 effective VOC in the glass container, connecting one arm of the olfactometer to this
954 treatment of n-hexane and blends of putative stimuli compounds and the other arm to
955 the controls (only n-hexane) (Supplementary Table 9). VOCs were passed from both
956 arms to the stem through equal flow rates of cleaned and humidified airflow created
957 by an air pump system with an activated charcoal filter and distilled water. To avoid

visual distractions to the pollinators, we placed the olfactometer in the center of a white table illuminated using three 40-W cool white fluorescent tubes above the arms.

Each healthy adult female pollinator (collected from figs in SCBG) was tested independently with an observation for 5 mins in the olfactometer, and its behavior was assigned to one of the three choices: (1) towards the treatment (the insect went 1 cm past the Y junction (decision line) and stayed there more than 1 min); (2) towards the control; and (3) no choice (the insect did not reach the decision line within 5 mins). For each treatment-control combination, we repeated this experiment 50 times (i.e. 50 adult female pollinators) and compared the proportions of different choices (towards the treatment and towards the control) using GLMs assuming binomial distribution of residuals to examine the preference of *W. pumilae*.

Sample collection for comparative transcriptome, proteome and metabolome. To reveal the molecular mechanisms forming the specific pollinator-host identification based on both transcriptomic and proteomic data, in spring 2017, after collecting several pre-receptive and receptive figs from the ten mature individuals of the plants used in VOCs collection (Supplementary Table 7), we dissected each sampled fig to gather ostiolar tissues with bracts. The total sample size therefore was 20 for the plant. In spring 2018, we sampled at least 5 figs at the mature stage from each of the five functional male mature individuals used for VOC collection (Supplementary Table 7). Each sampled mature fig was dissected into halves in a Teflon bag, and then each half was rapidly moved into a Teflon bag containing only clean air filtered by activated charcoal (as a control) or clean air and a receptive fig (as a treatment), to test whether

differential expression occurred in some chemosensory genes when adult females were exposed to attractive VOCs. We then collected all adult females of *W. pumilae* emerging from the sampled figs according to the identity of functional male trees (a total of 10 samples with at least 100 adult female wasps in each sample). All sampled fig tissues and adult female pollinators were first stored in liquid nitrogen for 72 hours and then moved into a refrigerator at -80 ℃.

To unravel how pollinator larvae adapt to the environments inside galled ovules using metabolomes, we sampled several receptive and post-receptive figs from the ten plant individuals (Supplementary Table 7) and collected ostiolar tissues (20 samples), female florets (10 samples), galled ovules (5 samples) and seeds (5 samples) in spring 2020. For clearly distinguishing galled ovules and seeds from the female florets that were neither pollinated nor utilized by pollinators, the post-receptive figs were sampled four weeks after the entrance of adult female pollinators.

RNA-seq for *F. pumila* var. *pumila* and *W. pumilae*. After generating PCR-based libraries and sequencing on a BGISEQ500 platform (BGI, CHN), low quality reads were filtered using SOAPnuke version 1.5.6[99]. The acquired clean reads were then mapped to the genome assemblies of our studied species using Bowtie version 2.2.5[100] and gene expression were quantified by RSEM version 1.2.12[101].

Quantitative proteomes for *F. pumila* var. *pumila* and *W. pumilae*. We identified and quantified proteins for ostiolar tissues (sampled in 2017) using iTRAQ (isobaric tags for relative and absolute quantitation)-based method. The strategy of quantifying

proteomes was conducted according to the methods described by Tian et al. (2013)[102]. After total protein extraction, peptide labeling was performed using an iTRAQ Reagent 8-plex Kit according to the manufacturer's protocol. Extraction was followed by peptide fractionation, and the peptides separated from LC-20AD nano-HPLC (Shimadzu, JPN) were transferred into the tandem mass spectrometry Q EXACTIVE (MS/MS) (Thermo Fisher Scientific, US) for data-dependent acquisition (DDA) detection. After converting the raw MS/MS data into MGF format using Proteome Discoverer version 1.2 (Thermo Fisher Scientific, US), the exported data in MGF format were searched using Mascot version 2.3 (Matrix Science, US) against the protein-coding sequences from our gene prediction. Quantification of proteins was achieved using IQuant[103], which uses the Mascot Percolator algorithm[104] to improve the results of peptide identification and the principle of parsimony to assemble proteomes. All the proteins with a false discovery rate (FDR)[105] of less than 1% were retained for further analyses.

We used a DIA (data independent acquisition) approach to identify and quantify proteins in adult female pollinators (collected in 2018). Procedures identical to iTRAQ were first performed on the total protein extraction, peptide fractionation and peptides separation. Then, to create reference spectra for DIA, we first conducted DDA on a Q-EXACTIVE HF mass spectrometer (Thermo Fisher Scientific, US) coupled with an Ultimate 3000 RSLCnano system (Thermo Fisher Scientific, US) after a further peptide separation on an in-house packed nano-LC column (150 μm × 30 cm, 1.8 μm, 100 Å). Then, using the same instruments, DIA was performed

following a brief procedure that consisted of a survey scan at 120,000 resolution from 400 to 1,250 m/z (MIT 50 ms), followed by scanning in DIA isolation windows setting17 m/z with loop count 50 at 30,000 resolution (automatic gain control target $3\times e^6$ and auto MIT). The DDA spectra were identified by searching against the database of protein-coding sequences using the MaxQuant version 1.5.3.30 [106](Cox and Mann, 2008) at the FDR level of 1% with the minimum peptide length of 7. Based on the spectrogram database of DDA spectra, peptides and proteins in DIA data were identified and quantified using Spectronaut[107], employing the mProphet approach and setting iRT for retention time prediction. A target-decoy model was used to verify the quantification results at an FDR level of 1%.

Measurement of metabolomes of different types of tissues. Chromatographic separation of metabolites was performed using an Ultra-Performance Liquid Chromatography (UPLC) System (Waters, UK), with an ACQUITY UPLC HSS T3 column (100mm*2.1mm, 1.8μm) (Waters, UK) being used for the reversed phase separation and setting oven temperature at 50° C and flow rate of 0.4 ml/min. After separation, gradient elution was conducted as following procedure: 0～2 min, 100% mobile phase A (water + 0.1% formic acid); 2~11 min, 0% to 100% mobile phase B (acetonitrile + 0.1% formic acid); 11~13 min, 100% B; 13~15 min, 0% to 100% A. The injection volume for each sample was 10 μl. Then, the eluted metabolites were identified in both positive and negative ion modes using a high-resolution tandem mass spectrometer Xevo G2 XS QTOF (Waters, UK). The capillary and sampling cone voltages were set at 3.0 kV and 40.0 V for positive ion mode and at 2.0 kV and

40.0 V for negative ion mode. Mass spectrometry data were acquired in Centroid MSE mode, setting the TOF mass range from 50 to 1200 Da and the scan time of 0.2 s. For MS/MS detection, all precursors were fragmented at 20-40 eV with the scan time of 0.2 s. A quality control (QC) sample (pooling all samples together) was used after every 10 samples. Peak alignment, peak picking and quantitation of each metabolite were performed using Progenesis QI version 2.2, and the quality control based on LOESS signal correction[108] was conducted using QC samples.

Comparative transcriptome, proteome and metabolome analysis. We carried out differential expression/concentration analysis for transcriptomes, proteomes and metabolomes, to detect the key genes contributing to the attractant-induced host specificity and the chemical cues for the adaptation of pollinator larvae to plant chemical defenses.

For transcriptomes, differential expression was tested in ostiolar tissues between the pre-receptive and the receptive stage. For the pollinator, differential expression was conducted between contacting attractive VOC(s) vs. not contacting and between adults and larvae. We performed comparisons using DEseq2 version 1.4.5[109] based on negative binomial distributions. *P*-values were corrected using a Benjamini-Hochberg (BH) method for multiple tests. The differentially expressed genes (DEGs) with a fold change ≥ 2 and an adjusted p-value ≤ 0.05 were considered as statistically significant.

For proteomes, we tested the proteins with significant difference in quantity (PSDs) in ostiolar tissues between the pre-receptive and the receptive stages and between sexes at each stage using IQuant, and PSDs were defined as fold changes in

protein abundance ≥ 1.2 and Q-value ≤ 0.05. In adult female pollinators, PSDs were analyzed using MSstats[110] at criterions of fold changes ≥ 2 and Q-value ≤ 0.05.

For metabolomes, to examine whether there were significant differences in profile of secondary metabolites associated with chemical defenses (SMCDs) between different types of tissues and between the receptive and the post-receptive stages, we first carried out enrichment analysis to enrich all relevant secondary metabolites into the pathways associated with plant chemical defenses and then clustered all samples into different categories using PLS-DA model in metaX[111]. Data were $\log_2$-transformed and scaled by Pareto scaling. Secondary metabolites with significant difference in quantity (SMSDs) were defined as VIP (variable importance for the projection calculated based on the first two axes from PLS-DA model) ≥1, fold change ≥ 1.2 or ≤ 0.83 and Q-value ≤ 0.05. In addition, we performed PLS-DA model to test the difference in the entire profile of secondary metabolites between different types of tissues and between different fig developmental stages.

Motif analysis. We conducted motif analysis to check whether the OBPs in the same syntenic blocks among the three pollinating wasp species have similar motif structure using MEME Suite 5.0.4[112]. Motifs with E-value ≤ 0.05 were used for inter-specific comparisons. To predict the most likely OBPs related to the identification of specific attractant and repellent, we created a dataset consisting of all OBPs in *W. pumilae* and the specific OBPs that had been verified to bind to decanal and nonanal in *Adelphocoris lineolatus*[33] and *Culex quinquefasciatus*[34] as references, and performed motif analysis.

***In vitro* functional characterization of key genes.** The full-length of open reading frame (ORF) of the four key genes (for the plant) and of the two OBPs (for the pollinator) (Supplementary Table 17) was confirmed by RT–PCR and was then cloned into pET-28a (MilliporeSigma, US). After checking sequences by Sanger sequencing, these genes were expressed in *E. coli* strains BL21 (DE3) and Rosetta (DE3). The recombinant proteins produced were purified (purity > 90%) using modified nickel-nitrilotriacetic acid agarose (Thermo Fisher Scientific, US).

We measured the affinities of the two OBPs to different substrates using surface plasmon resonance (SPR) on a Biacore T200 system (GE Healthcare). OBPs were reconstituted in sterile PBS and were diluted in 10mM sodium acetate trihydrate (pH = 4.5) to the concentration of 20ug/ml. Then, each OBP was immobilized by the amine coupling method on a CM5 sensor chip according to the manufacturer's protocol (GE Healthcare). Analytes (decanal and nonanal) were diluted in running buffer (5% DMSO-PBS-P) to the concentration ranging from 0 to 1000 μM and were injected through channels at a flow rate of 20 μl/min. Using BIAevaluation (GE Healthcare), both steady state affinity model and 1:1 binding model were performed to quantify the binding affinity (K_D).

For enzyme activity assays of the four key genes of the plant, we used the reaction system (500 μl) mainly composed of 50 mM Tris-HCl (pH 7.4), 0.4~1.0 mM substrate(s) (Supplementary Table 17), 2M dimethyl sulfoxide (for the ADH and the ALDH)/10% triton X-100 (for the two ASCLs), and 10 μl of purified protein (0.2 mg/ml). After 60 min of incubation at room temperature, we collected the reaction

products by headspace solid-phase microextraction for the ALDH and the ADH (which were analyzed by GC–MS) and by extraction using diethyl ether for the two ACSLs (which were analyzed by LC–MS). These experiments were repeated for three time. In addition, three replications of negative controls (only adding the subtrates and bovine serum albumin) were conducted, and no reaction products were detected.

Cis-element detection and co-expression network analysis. To test the regulatory mechanisms in the biosynthesis of attractant and repellent emitted by figs of *F. pumila* var. *pumila*, we first scanned the binding motifs present in the 2-kb promoter sequences upstream of key plant genes using PlantCARE[116]. Then, weighted undirected co-expression networks were conducted using the R package WGCNA[113] with a soft thresholding power of 8. Modules containing genes with correlated expression patterns were identified by gene clustering based on the topological overlap matrix[114] and by cutting the resulting dendrogram using the cutreeDynamic approach in the R package The Dynamic Tree Cut[115]. Genes with kME values larger than 0.95 were selected as hub genes. We checked whether some modules containing both some key plant genes and the transcription factors predicted to bind to them. This allowed us to uncover the likely regulatory mechanisms.

ChIP-qPCR. The open reading frame of each of the four transcription factors (*FpumHD-ZIP1*, *FpumHD-ZIP2*, *FpumbZIP1* and *FpumbHLH1* (Supplementary Table 13)) was cloned into the pET-28a to generate the fusion plasmid encoding the 6 His-tagged fusion protein. This plasmid was transformed into *E. coli* strain Rosetta

(DE3), which were cultured and induced by 0.8 mM isopropyl-β-D-thiogalactoside (IPTG) at 37 °C. The induced cells were then sonicated for supernatant collection, and the purified recombinant proteins were obtained using a His-tag Protein Purification Kit (Beyotime Biotechnology, CHN). The purified proteins were used to immunize rabbits for 52 days to acquire polyclonal antibody (ABclonal Biotechnology, CHN). We successfully obtained the qualified antibodies for all the four transcription factors for ChIP-qPCR experiments.

ChIP-qPCRs were then conducted for the two transcription factors with qualified antibodies to examine if it can bind the putative target genes by model prediction. The ChIP assay was performed based on the protocols described in Gendrel et al., (2005)[117]. Approximately 3.0 g ostiolar tissues from figs at receptive stages were treated using 1% formaldehyde to crosslink and fix the DNA-protein complexes. The cells of sampled tissues were lysed, and each antibody was used to immunoprecipitate the antigen transcription factor with its binding DNA fragments. The DNA in the ChIP products was applied in qPCR with primer pairs designed for the promoters of putative target genes in a QuantStudio™ 5 real-time PCR detection system (Thermo Fisher Scientific, US). Each qPCR reaction was performed in triplicates, and the cycle thresholds (Cts values) of ChIP products were compared with those of input samples and negative controls (only using IgG) for calculating % input and fold enrichment (% input (ChIP)/ % input (negative control)). We failed to obtain the Ct values for negative controls by the end of 35 qPCR cycles, and we therefore used the Ct value of 35 for each negative control when calculating % input and fold enrichment.

Data availability

The data that support the findings of this study have been deposited in the CNSA (https://db.cngb.org/cnsa/) of CNGBdb with accession code CNP0000674.

Code availability

All analyses in this study were conducted using published programs, and all codes for data analysis are provided in Methods.

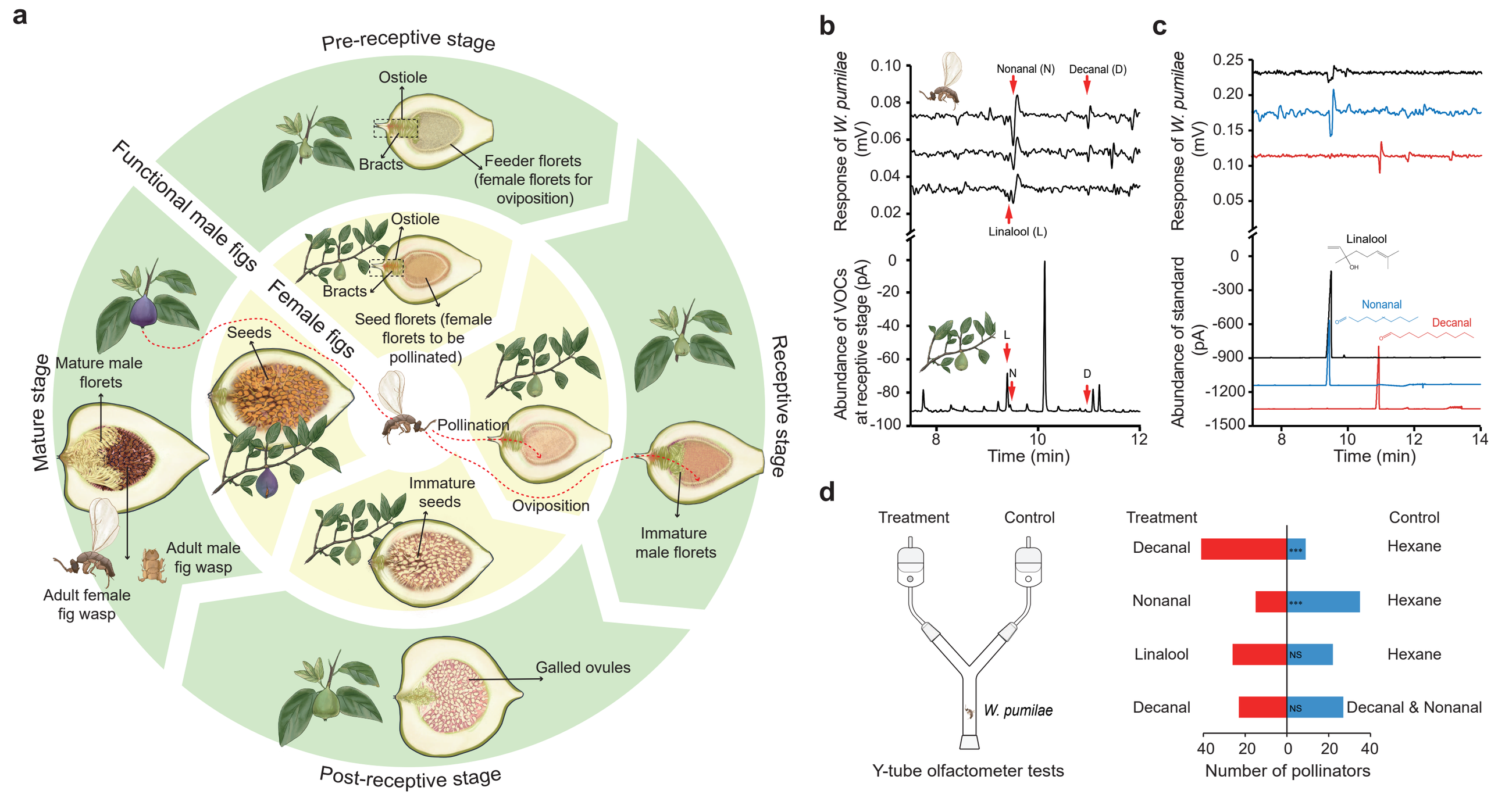
a
Pre-receptive stage
Ostiole
Bracts
Feeder florets (female florets for oviposition)
Functional male figs
Female figs
Ostiole
Bracts
Seed florets (female florets to be pollinated)
Seeds
Mature male florets
Mature stage
Pollination
Oviposition
Immature seeds
Receptive stage
Immature male florets
Adult male fig wasp
Adult female fig wasp
Galled ovules
Post-receptive stage
b
Response of W. pumilae (mV)
Nonanal (N)
Decanal (D)
Linalool (L)
Abundance of VOCs at receptive stage (pA)
L
N
D
Time (min)
c
Response of W. pumilae (mV)
Linalool
Nonanal
Decanal
Abundance of standard (pA)
Time (min)
d
Treatment
Control
W. pumilae
Y-tube olfactometer tests
Treatment
Control
Decanal
Hexane
Nonanal
Hexane
Linalool
Hexane
Decanal
Decanal & Nonanal
***
***
NS
NS
Number of pollinators

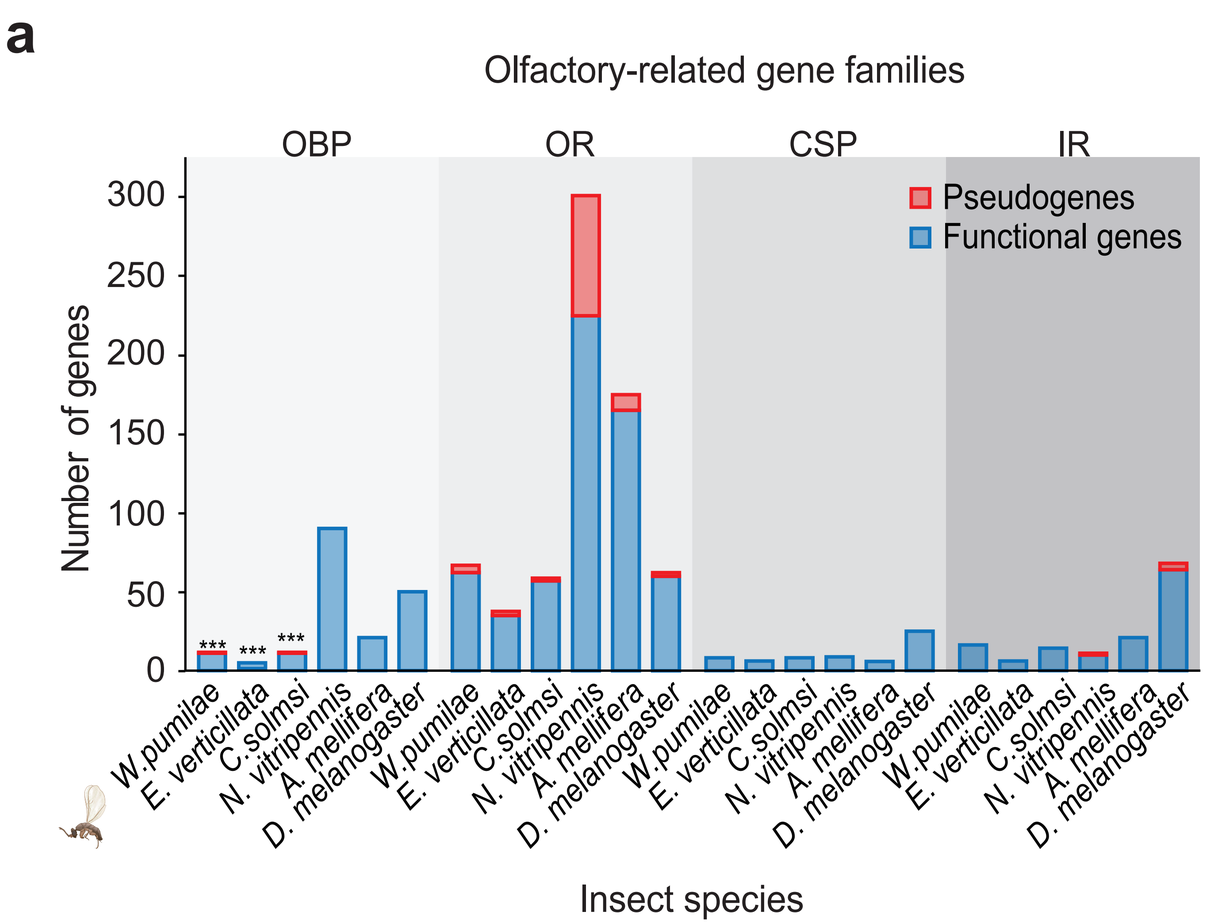
a
Olfactory-related gene families
OBP
OR
CSP
IR
Pseudogenes
Functional genes
Number of genes
300
250
200
150
100
50
0
***
***
***
W.pumilae
E. verticillata
C.solmsi
N. vitripennis
A. mellifera
D. melanogaster
Insect species

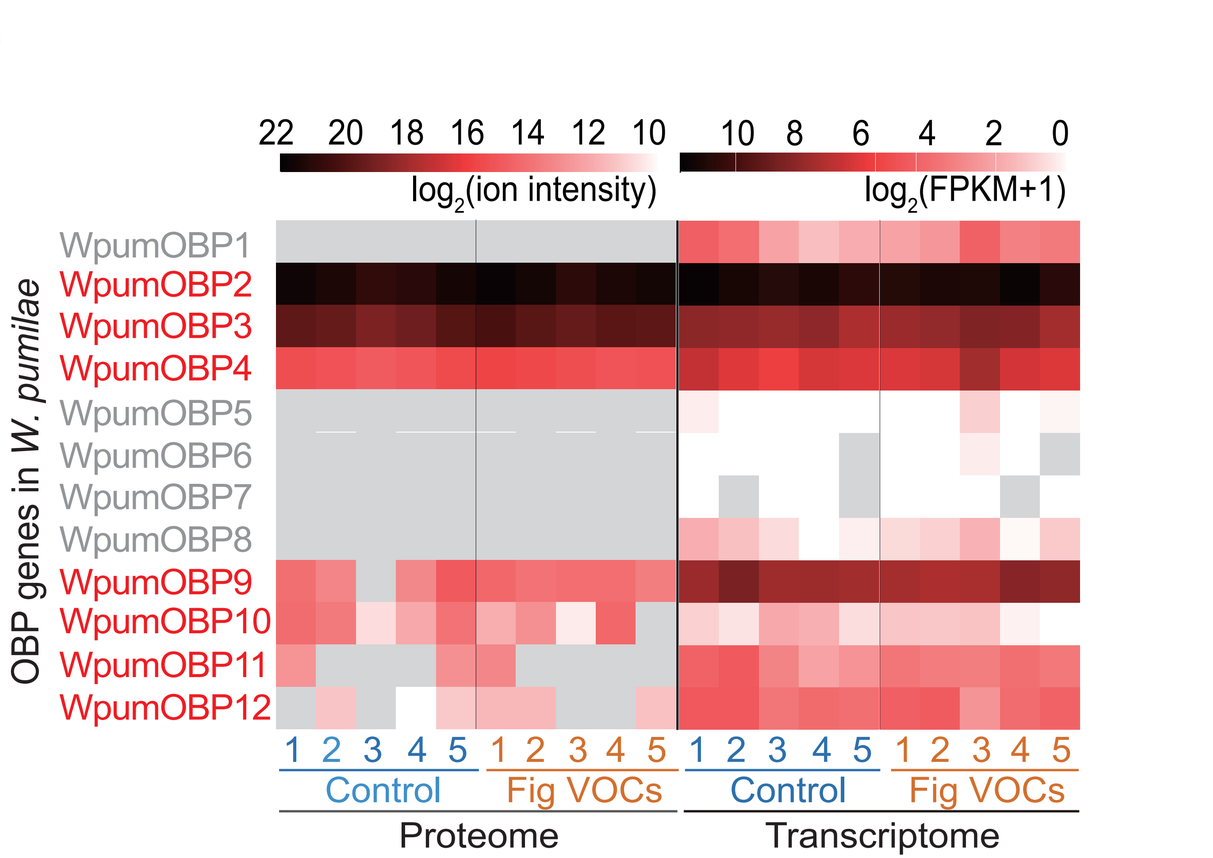
b
22 20 18 16 14 12 10
log2(ion intensity)
10 8 6 4 2 0
log2(FPKM+1)
OBP genes in W. pumilae
WpumOBP1
WpumOBP2
WpumOBP3
WpumOBP4
WpumOBP5
WpumOBP6
WpumOBP7
WpumOBP8
WpumOBP9
WpumOBP10
WpumOBP11
WpumOBP12
1 2 3 4 5 1 2 3 4 5
Control
Fig VOCs
Proteome
1 2 3 4 5 1 2 3 4 5
Control
Fig VOCs
Transcriptome

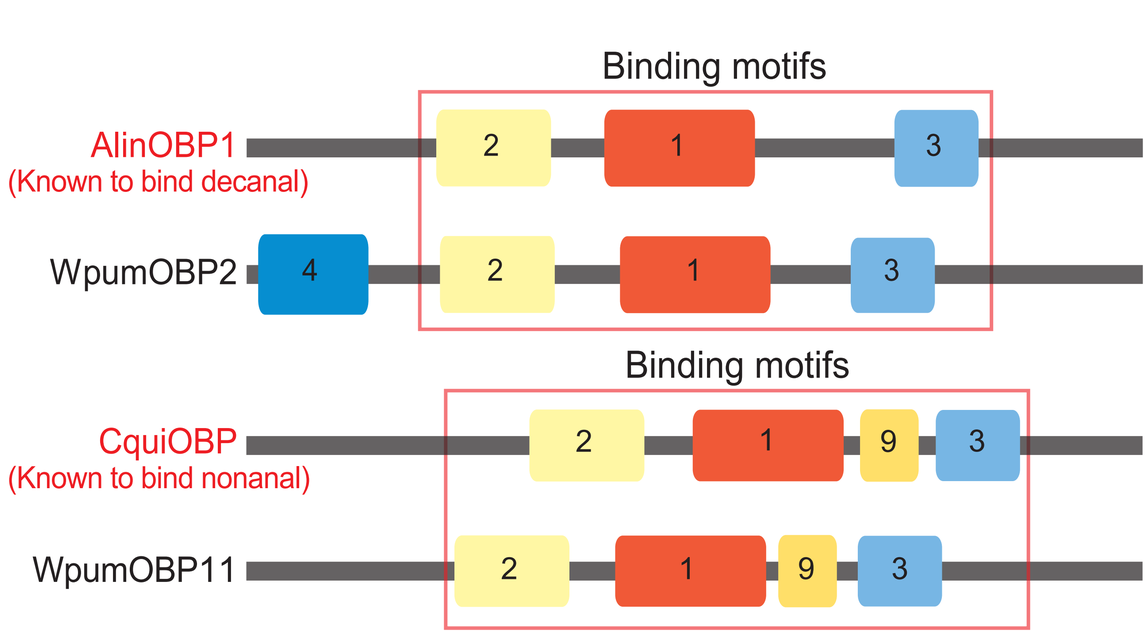
c
Binding motifs
AlinOBP1
(Known to bind decanal)
2
1
3
WpumOBP2
4
2
1
3
Binding motifs
CquiOBP
(Known to bind nonanal)
2
1
9
3
WpumOBP11
2
1
9
3

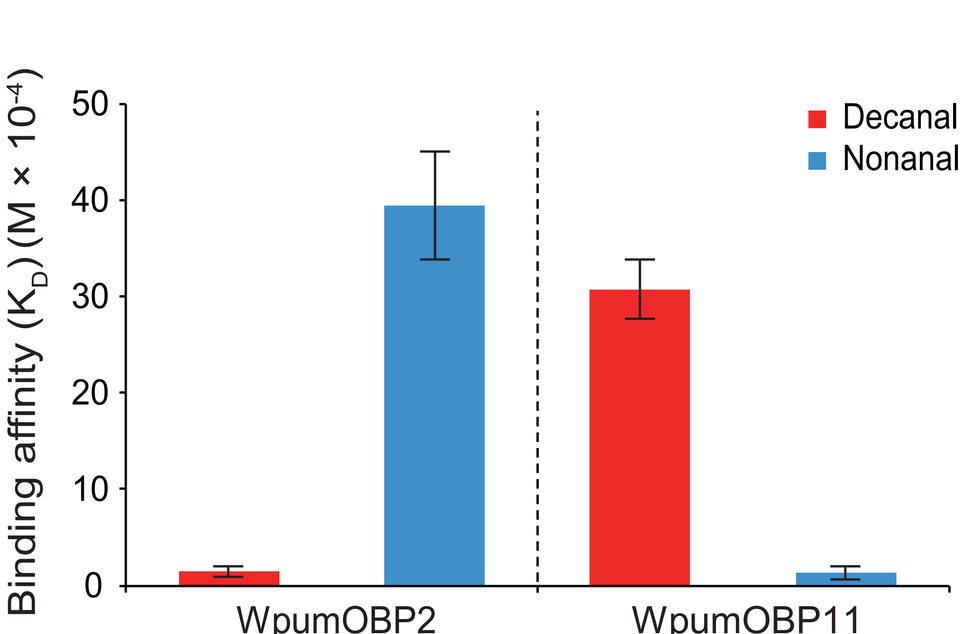
d
Binding affinity (KD) (M × 10-4)
50
40
30
20
10
0
Decanal
Nonanal
WpumOBP2
WpumOBP11

a

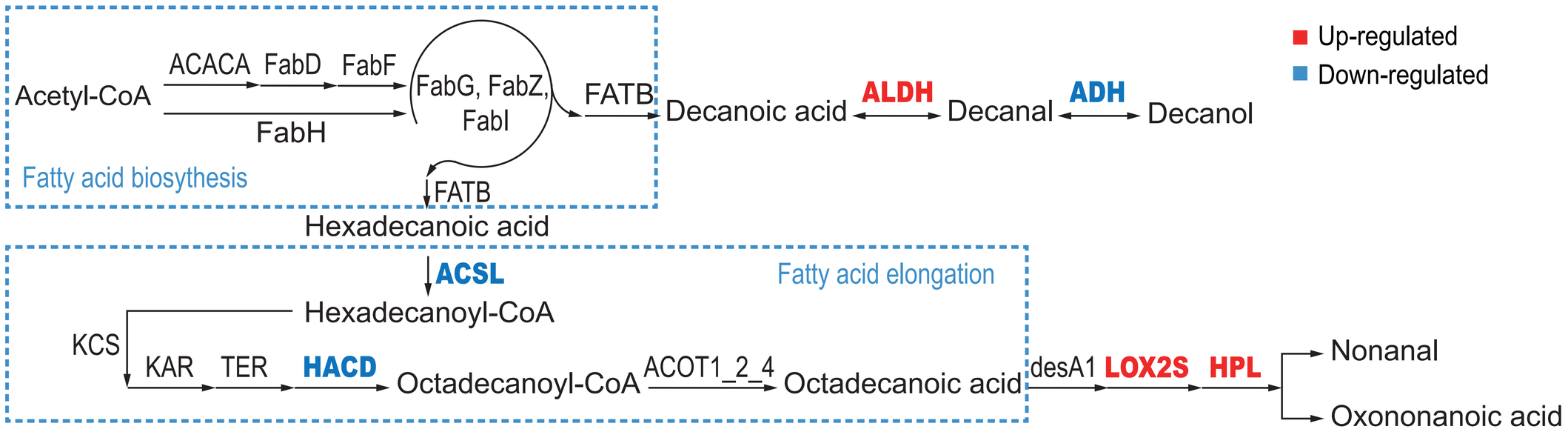
Up-regulated
Down-regulated
Acetyl-CoA
ACACA FabD FabF
FabH
FabG, FabZ, FabI
FATB
Fatty acid biosythesis
Decanoic acid
ALDH
Decanal
ADH
Decanol
FATB
Hexadecanoic acid
ACSL
Fatty acid elongation
Hexadecanoyl-CoA
KCS
KAR TER HACD
Octadecanoyl-CoA
ACOT1_2_4
Octadecanoic acid
desA1 LOX2S HPL
Nonanal
Oxononanoic acid

b

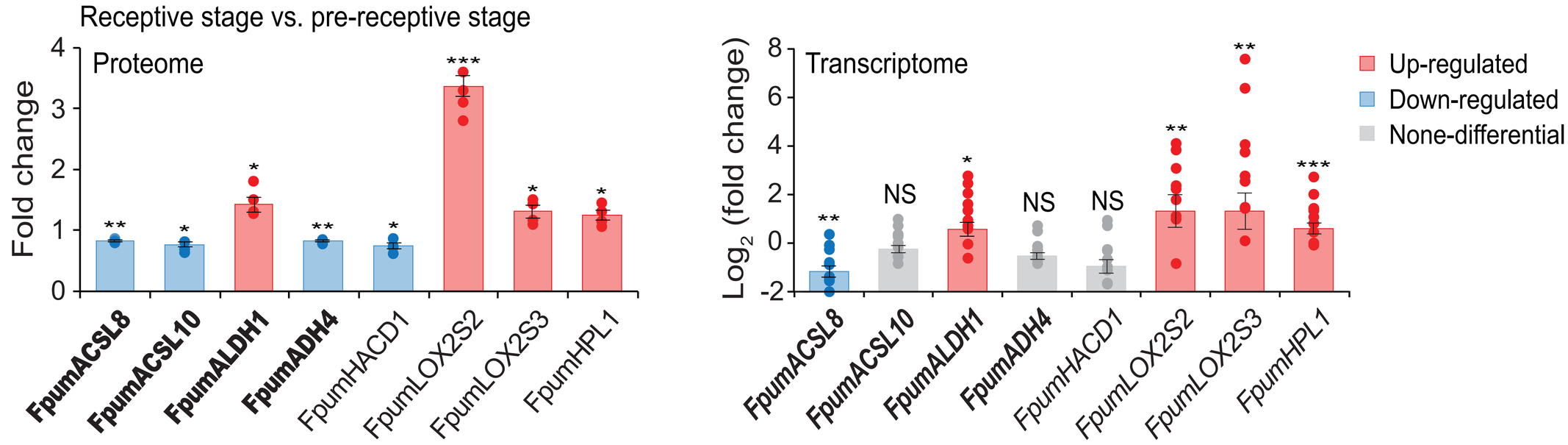
Receptive stage vs. pre-receptive stage
Proteome
Fold change
Transcriptome
Log2 (fold change)
Up-regulated
Down-regulated
None-differential
NS
FpumACSL8
FpumACSL10
FpumALDH1
FpumADH4
FpumHACD1
FpumLOX2S2
FpumLOX2S3
FpumHPL1

c

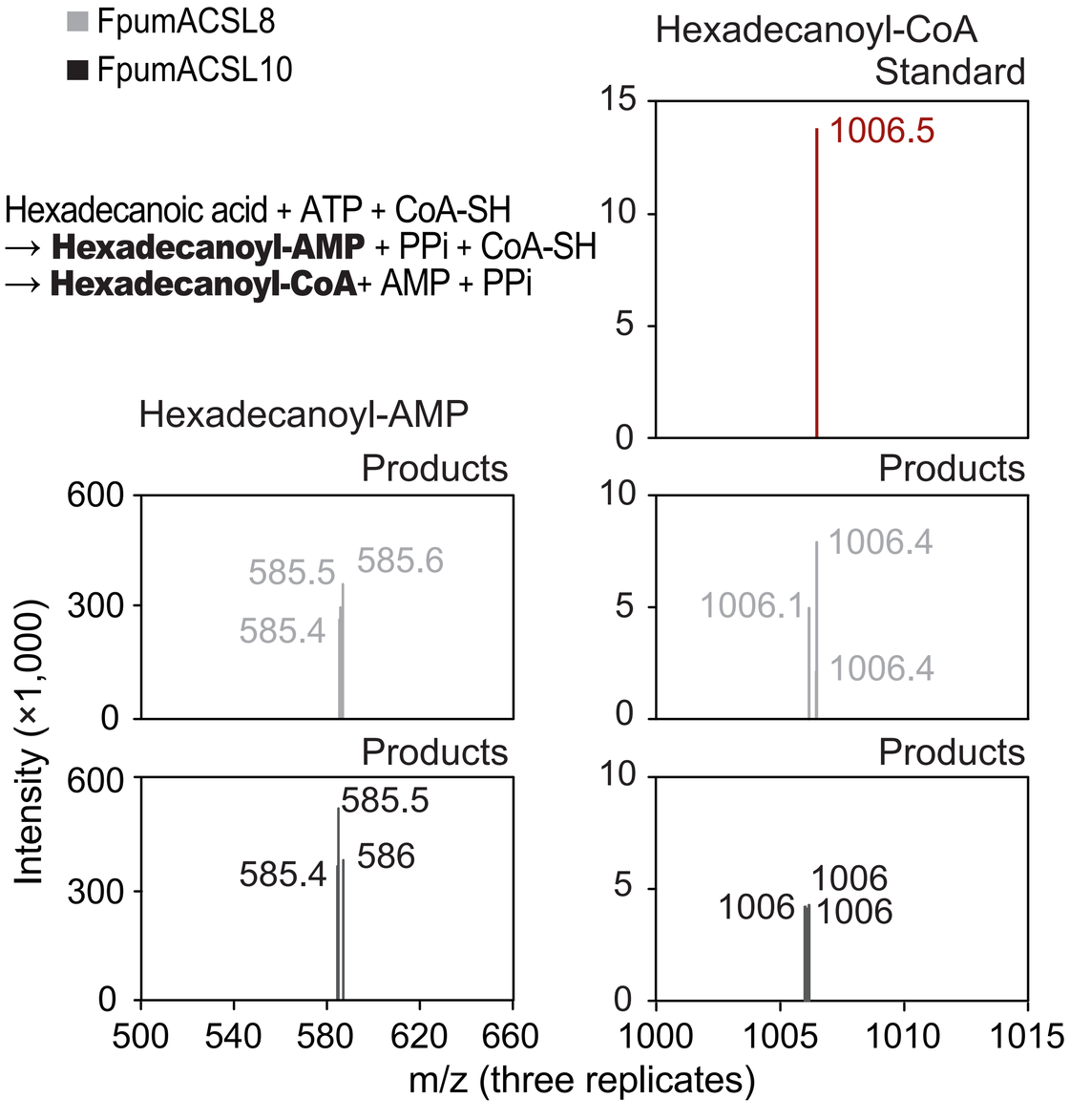
FpumACSL8
FpumACSL10
Hexadecanoic acid + ATP + CoA-SH
→ Hexadecanoyl-AMP + PPi + CoA-SH
→ Hexadecanoyl-CoA + AMP + PPi
Hexadecanoyl-CoA
Standard
1006.5
Hexadecanoyl-AMP
Products
585.5
585.6
585.4
1006.4
1006.1
586
1006
Intensity (×1,000)
m/z (three replicates)

d

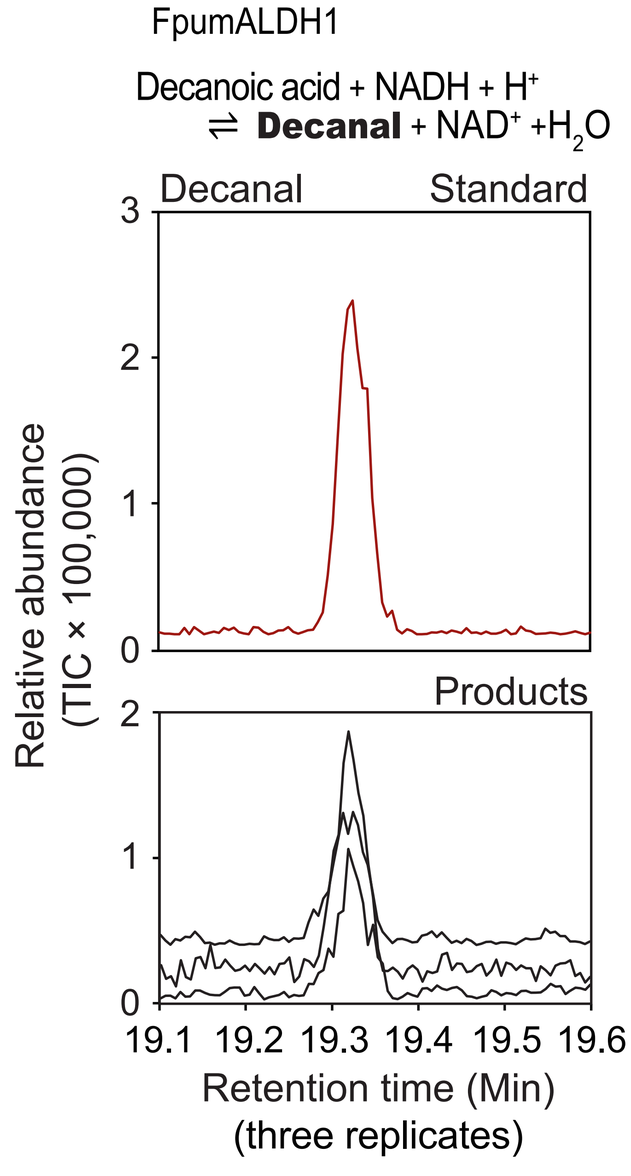
FpumALDH1
Decanoic acid + NADH + H+
⇌ Decanal + NAD+ +H2O
Decanal
Standard
Products
Relative abundance
(TIC × 100,000)
Retention time (Min)
(three replicates)

e

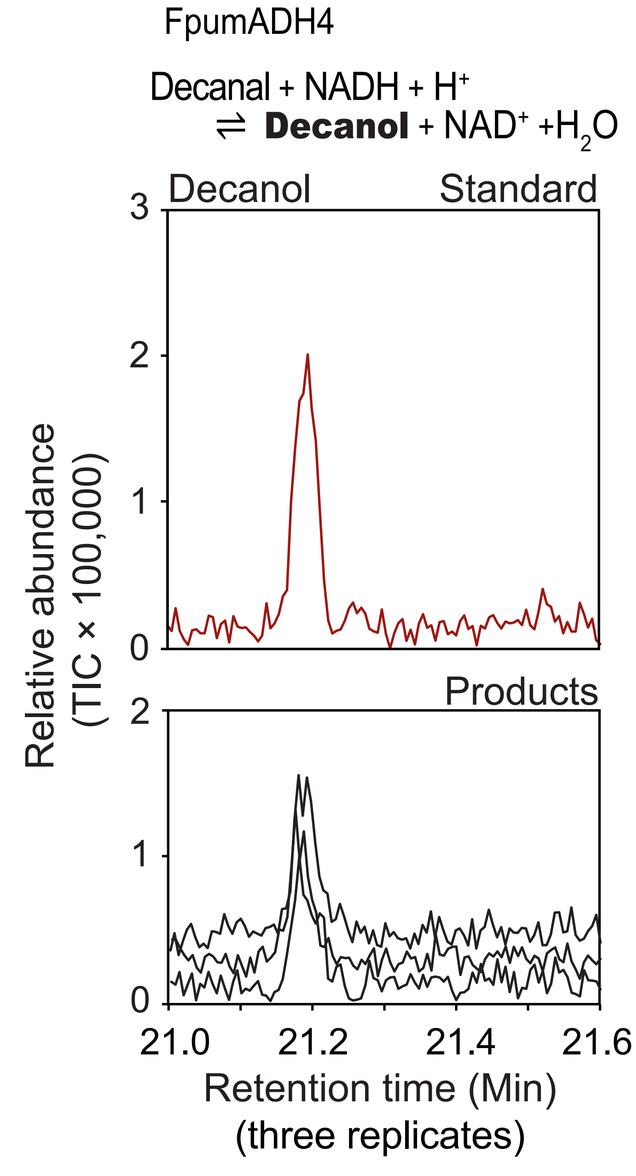
FpumADH4
Decanal + NADH + H+
⇌ Decanol + NAD+ +H2O
Decanol
Standard
Products
Relative abundance
(TIC × 100,000)
Retention time (Min)
(three replicates)

f

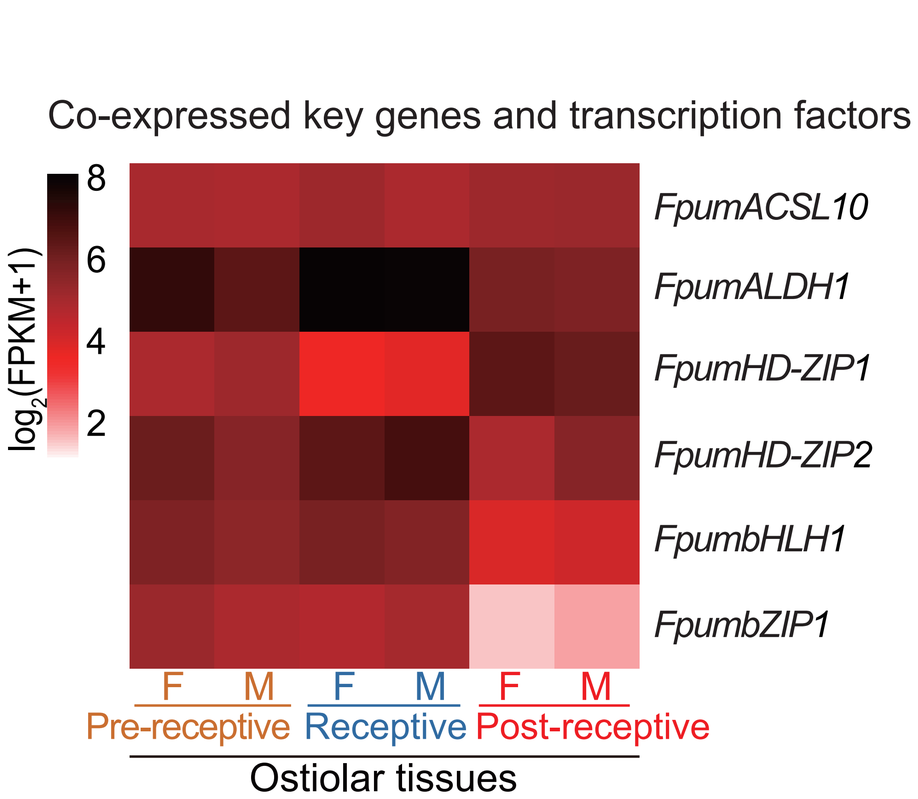
Co-expressed key genes and transcription factors
log2(FPKM+1)
FpumACSL10
FpumALDH1
FpumHD-ZIP1
FpumHD-ZIP2
FpumbHLH1
FpumbZIP1
F M F M F M
Pre-receptive Receptive Post-receptive
Ostiolar tissues

g

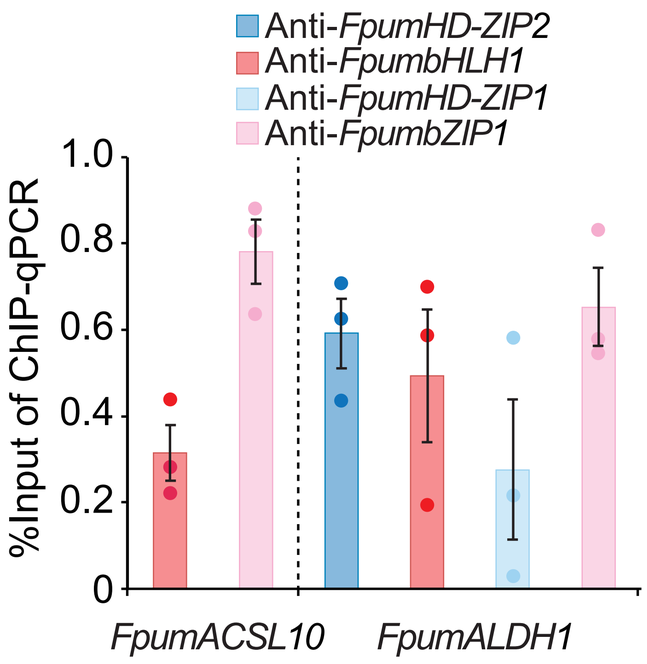
Anti-FpumHD-ZIP2
Anti-FpumbHLH1
Anti-FpumHD-ZIP1
Anti-FpumbZIP1
%Input of ChIP-qPCR
FpumACSL10
FpumALDH1

h

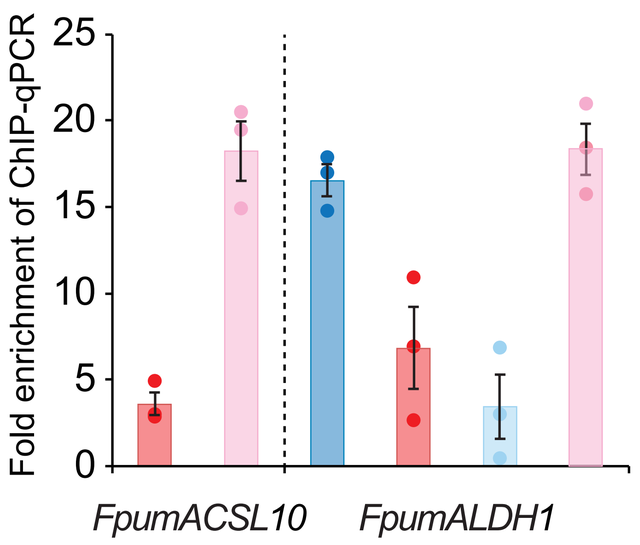
Fold enrichment of ChIP-qPCR
FpumACSL10
FpumALDH1

a

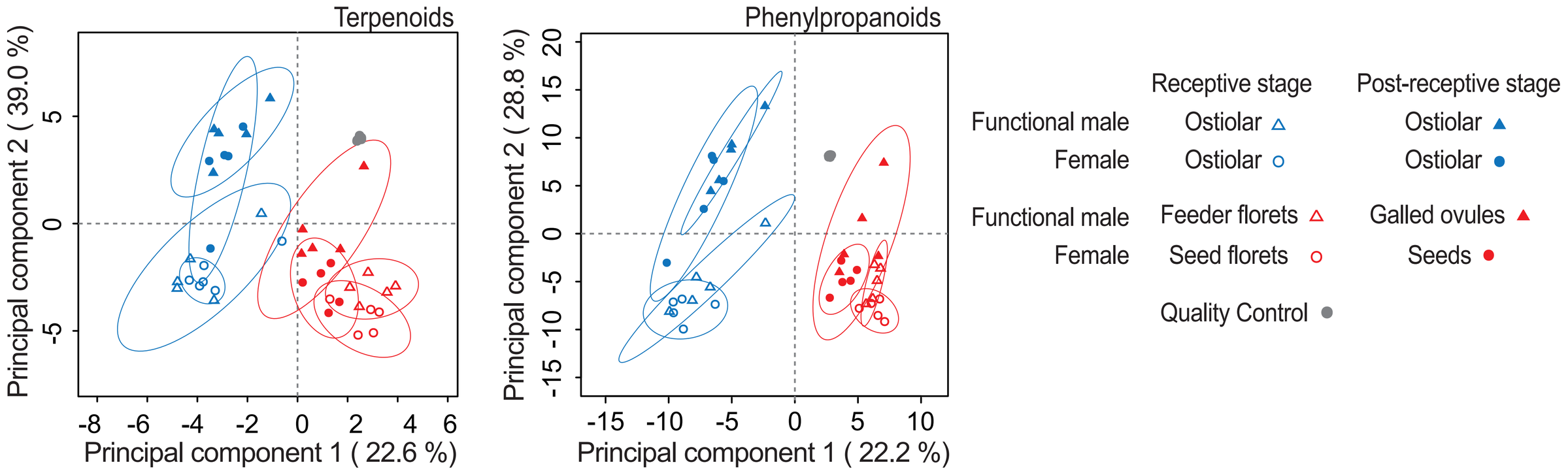
Terpenoids
Principal component 2 (39.0 %)
Principal component 1 (22.6 %)
Phenylpropanoids
Principal component 2 (28.8 %)
Principal component 1 (22.2 %)
Receptive stage
Post-receptive stage
Functional male
Ostiolar
Ostiolar
Female
Ostiolar
Ostiolar
Functional male
Feeder florets
Galled ovules
Female
Seed florets
Seeds
Quality Control

b

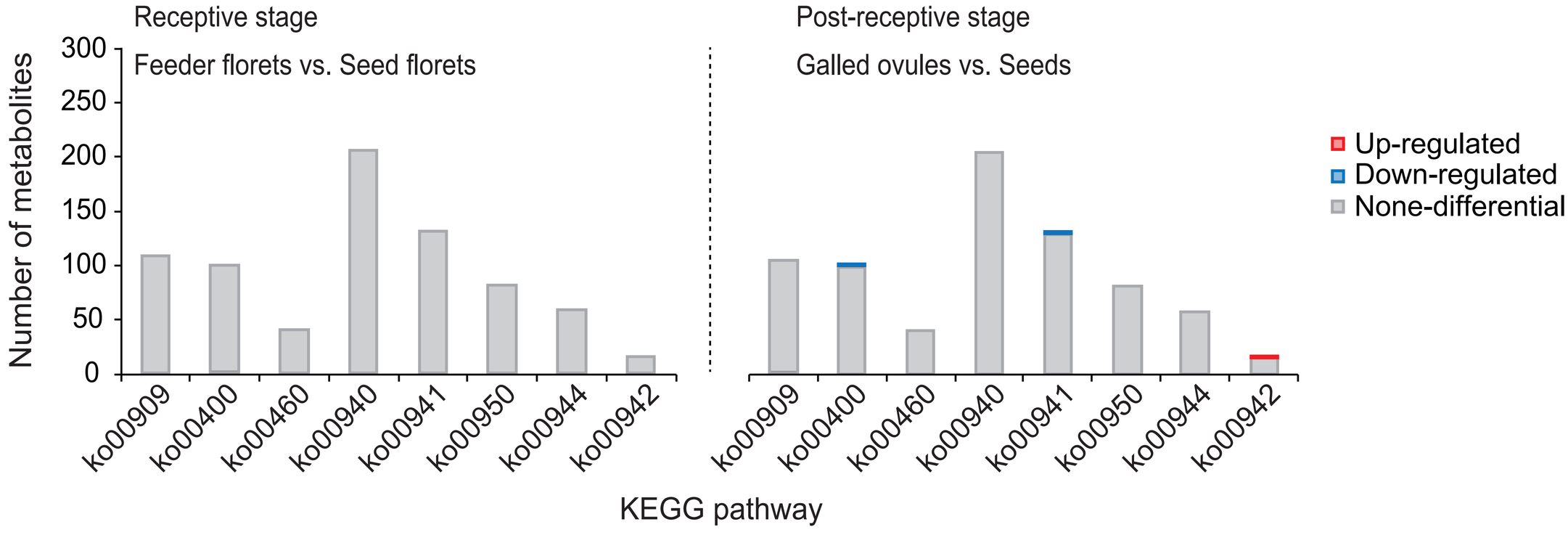
Receptive stage
Feeder florets vs. Seed florets
Post-receptive stage
Galled ovules vs. Seeds
Number of metabolites
ko00909
ko00400
ko00460
ko00940
ko00941
ko00950
ko00944
ko00942
KEGG pathway
Up-regulated
Down-regulated
None-differential

c

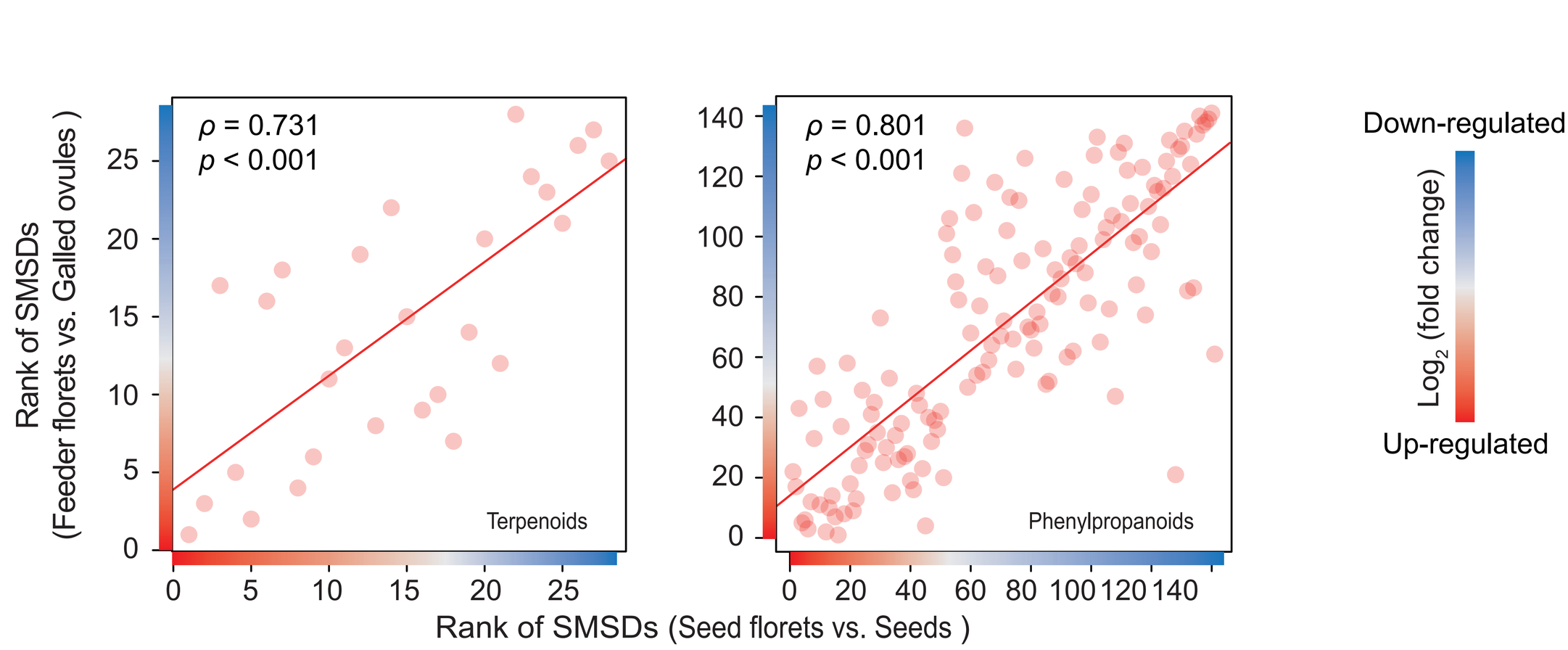
Rank of SMSDs
(Feeder florets vs. Galled ovules)
ρ = 0.731
p < 0.001
Terpenoids
ρ = 0.801
p < 0.001
Phenylpropanoids
Rank of SMSDs (Seed florets vs. Seeds)
Down-regulated
Log2 (fold change)
Up-regulated

d

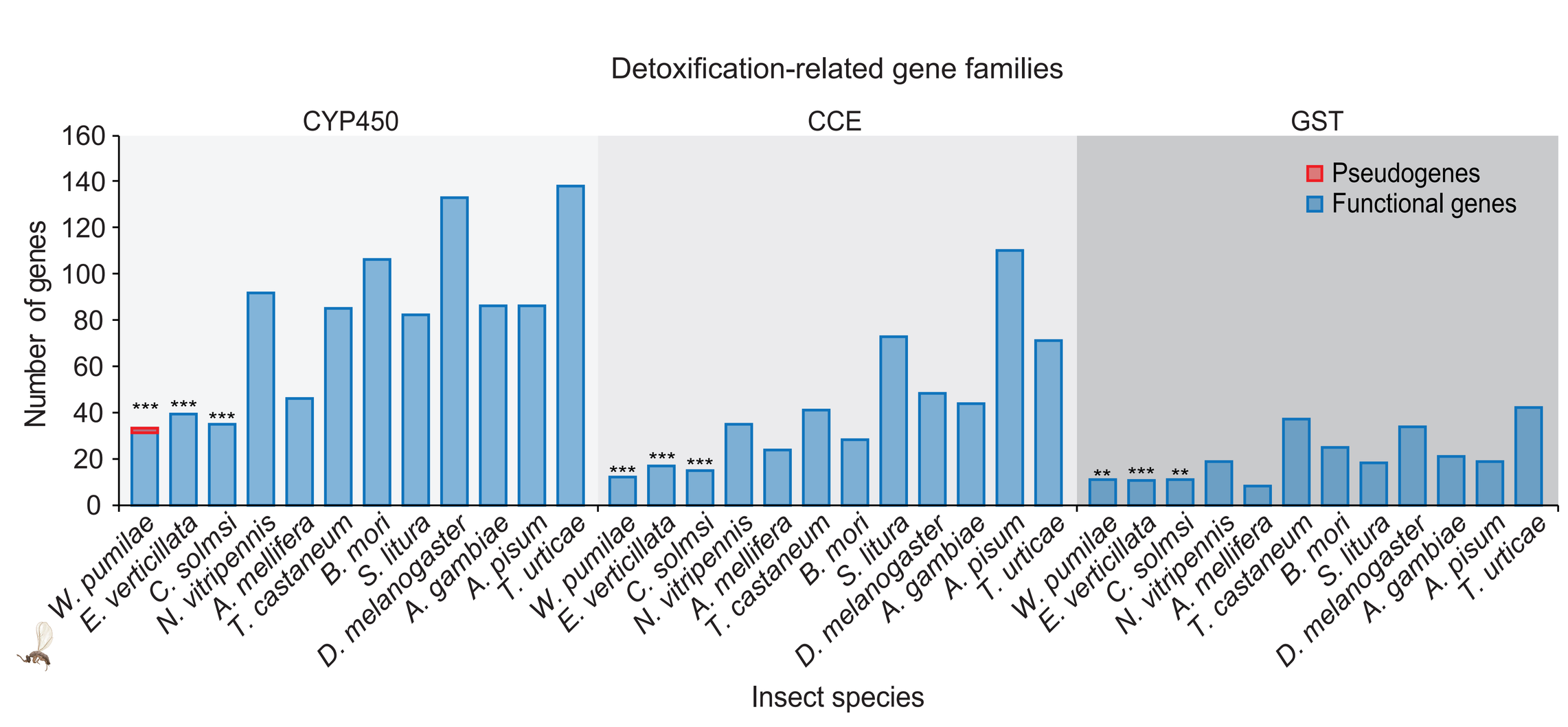
Detoxification-related gene families
CYP450
CCE
GST
Pseudogenes
Functional genes
Number of genes
W. pumilae
E. verticillata
C. solmsi
N. vitripennis
A. mellifera
T. castaneum
B. mori
S. litura
D. melanogaster
A. gambiae
A. pisum
T. urticae
Insect species